A lateral protrusion latticework connects neuroepithelial cells and is regulated during neurogenesis

Ioannis Kasioulis[1], Alwyn Dady, John James[2,3], Alan Prescott[2],

Pamela A. Halley & Kate G. Storey*

Division of Cell & Developmental Biology, School of Life Sciences,

University of Dundee, Dundee DD1 5EH, UK

[1] Current address, Department of Clinical Neurosciences, University of Cambridge
[2] Dundee Imaging Facility, School of Life Sciences
[3] Posthumous
* Corresponding author

Key words: developing neuroepithelium, apical endfeet, cell protrusions, actin dynamics, live imaging

Running title: Lateral protrusion latticework

Abstract

Dynamic contacts between cells within the developing neuroepithelium are poorly understood but play important roles in cell and tissue morphology and cell signalling. Here, using live-cell imaging and electron microscopy we reveal multiple protrusive structures in neuroepithelial apical endfeet of the chick embryonic spinal cord, including sub-apical protrusions that extend laterally within the tissue, and observe similar structures in human neuroepithelium. We characterise the dynamics, shape, and cytoskeleton of these lateral protrusions and distinguish these structures from cytonemes/filopodia and tunnelling nanotubes. We demonstrate that lateral protrusions form a latticework of membrane contacts between non-adjacent cells, depend on actin but not microtubule dynamics and provide a lamellipodial-like platform for further extending fine actin-dependent filipodia. We find that lateral protrusions depend on the actin-binding protein WAVE1: mutant-WAVE1 misexpression attenuated protrusion and generated a round-ended apical endfoot morphology. However, this did not alter apico-basal cell polarity nor reduce tissue integrity. During normal neuronal delamination sub-apical protrusions were withdrawn, but mutant-WAVE1-induced precocious protrusion loss was insufficient to trigger neurogenesis. This study uncovers a new form of cell-cell contact within the developing neuroepithelium regulation of which prefigures neuronal delamination.

Introduction

The patterning and production of differentiating cells within a proliferative epithelium is a central activity in tissue homeostasis and embryonic development. Recent advances have identified roles for cellular protrusions in these processes in a range of tissues including epithelia (Gerdes and Pepperkok, 2013; González-Méndez et al., 2019; Mattes and Scholpp, 2018). It is now clear that there are many types of cellular protrusion and that these vary in dimension, dynamics and involvement of specific cytoskeletal components. Such protrusions can also be distinguished by whether their protrusive behaviour results in cell-to-cell membrane contact, as exhibited by cytonemes/filopodia (Ramírez-Weber and Kornberg, 1999) or connection and the sharing of cytoplasmic content, including small organelles, characteristic of tunnelling nanotubes (Rustom et al., 2004). Cytonemes are long, fine, actin-dependent filopodia which can contact cells up to several hundred microns away and were first shown to mediate signalling at a distance in *Drosophila* (Cohen et al., 2010; De Joussineau et al., 2003; Hsiung et al., 2005; Rajan et al., 2009). Since then, a plethora of similar cellular protrusions, some containing microtubules at their base, have been described in other embryos and their functional significance is beginning to be elucidated (González-Méndez et al., 2019). In the developing vertebrate nervous system, this has been most closely addressed in zebrafish. Here fine actin-dependent filopodia deliver Wnt ligand to pattern the neural plate (Luz et al., 2014; Mattes et al., 2018; Stanganello et al., 2015). Later, in the neural tube, the Notch ligand Delta, is presented by transient basally originating cell protrusions produced by newborn neurons to regulate the spatial and temporal production for spinal cord neurons (Hadjivasiliou et al., 2019). A correlation between filopodia and Notch ligand presentation has also been identified in the mouse cortex (Moore et al., 2020; Nelson et al., 2013), while other work supports a dependence on apical adherens junction localised Notch ligands in chick and mouse neuroepithelium (Hatakeyama et al., 2014). The former findings with respect to Wnt signalling and others reporting presentation of further ligands or their receptors, including Sonic hedgehog, Bone morphogenetic protein and Fibroblast growth factor, in non-neural contexts (Huang et al., 2019; Roy et al., 2014; Sanders et al., 2013) raise an alternative or complementary hypothesis to the notion that signal diffusion through extracellular space underlies establishment of signalling gradients which pattern developing tissues (Briscoe and Small, 2015; Kornberg, 2014; Wolpert, 2016). Whether similar cell protrusions exist and mediate patterning and neuronal differentiation or confer mechanical properties in the developing neuroepithelium in other model vertebrates or in human tissue has yet to be determined.

In the adult nervous system, cellular protrusions have been proposed to mediate pathogen spread in the form of prions and to facilitate progression of neurodegenerative diseases such as Alzheimer's (Victoria and Zurzolo, 2017). A further related possibility is that cell protrusions propagate infectious agents within the developing neuroepithelium. These considerations highlight the

importance of elucidating protrusive cell behaviour particularly at the apical surface of the neuroepithelium which is exposed to the fluid filled ventricle of the neural tube. The apical surface is made by the apical endfeet of neuroepithelial cells, which are linked together by N-Cadherin containing adherens junctions, essential for cell adhesion and tissue integrity (Hatta and Takeichi, 1986; Kadowaki et al., 2007; Meng and Takeichi, 2009). The pseudostratified nature of the neuroepithelium is characterised by interkinetic nuclear migration as neural progenitors progress through the cell cycle and divide at the apical surface (Miyata, 2008; Sauer, 1935). Within this proliferating cell population individual cells are then selected for neuronal differentiation by rising proneural gene expression and lateral inhibition mediated by Notch-Delta signalling (Henrique et al., 1995; Henrique and Schweisguth, 2019). Importantly, the transcription factor cascade that drives neuronal differentiation regulates the expression of *Cadherins* (Itoh et al., 2013; Rousso et al., 2012), reduction of which impacts adherens junctions and the linked intra-cellular actin network in the apical endfoot. These steps prefigure the delamination of newborn neurons from the ventricular surface in a process that involves local actin and microtubule cytoskeletal re-configuration (Camargo Ortega et al., 2019; Kasioulis and Storey, 2018; Kawaguchi, 2020) and in the chick and mouse neural tube, abscission of the apical membrane and dismantling of primary cilium (Das and Storey, 2014; Kasioulis et al., 2017), reviewed in (Kasioulis and Storey, 2018; Paridaen and Huttner, 2014). The presence of apical microvilli has been documented using electron microscopy (Shepard et al., 1997, 1993; Smith et al., 1982; Waterman, 1976) and immunofluorescence (Marzesco et al., 2005; Weigmann et al., 1997). Recent analyses have also identified sub-apical protrusions implicated in tissue elasticity underlying interkinetic nuclear migration (Shinoda et al., 2018). However, detailed characterization of the range of protrusive structures at the apical surface and extending sub-apically within the vertebrate neuroepithelium using live imaging approaches has yet to be undertaken.

Here we take advantage of the ability to transfect a mosaic of neuroepithelial cells in the chicken embryonic spinal cord to live image and monitor apical and sub-apical protrusion dimensions and dynamics. We further use electron microscopy to document apical endfoot protrusions in chicken and human neuroepithelium. Focusing on lamellipodia-like sub-apical lateral protrusions we parametrize these structures and demonstrate that they extend over several endfoot diameters and meet protrusions of non-neighbouring cells. Moreover, sub-apical lateral protrusions provided a platform for extension of fine filopodia, which we distinguish from cytonemes and tunnelling nanotubes. Distinct configurations of actin networks are regulated by distinct actin nucleating proteins of the WAVE family (Campellone and Welch, 2010; Sweeney et al., 2015; Yamazaki et al., 2005) and we show here that sub-apical lateral protrusions depend on WAVE1. We investigate the functional consequences of WAVE1 manipulation and identify a role for the regulation of the WAVE1-mediated actin network in neuronal delamination.

Results

Multiple protrusive structures emerge from neuroepithelial apical endfeet

To investigate the ultra-structural of neuroepithelial apical endfeet we used transmission electron microscopy (TEM), generating thin transverse sections of spinal cord (interlimb region) from chicken (HH stage 12) (Figures 1 A-C) and human (CS12) embryos (Figure 1D). This revealed key features in serial sections of the chicken tissue, including lumen protruding primary cilia (asterisks) and microvilli with a range of morphologies (blue arrowheads) (Figures 1 A-C). Focussing on contacts between neuroepithelial cells we identified thin plasma membrane that spread between adjacent endfeet (black arrow heads Figure 1C) apical to adherens junctions (white arrowheads), and sub-apical membrane protrusions (yellow arrowheads) that extend laterally over neighbouring cells below adherens junctions. These key sub-cellular structures could also be identified in human tissue (Figure 1D), which was distinguished by the presence of extensive microvilli, sub-apical lateral protrusions and prominent mitochondria (pink arrowheads).

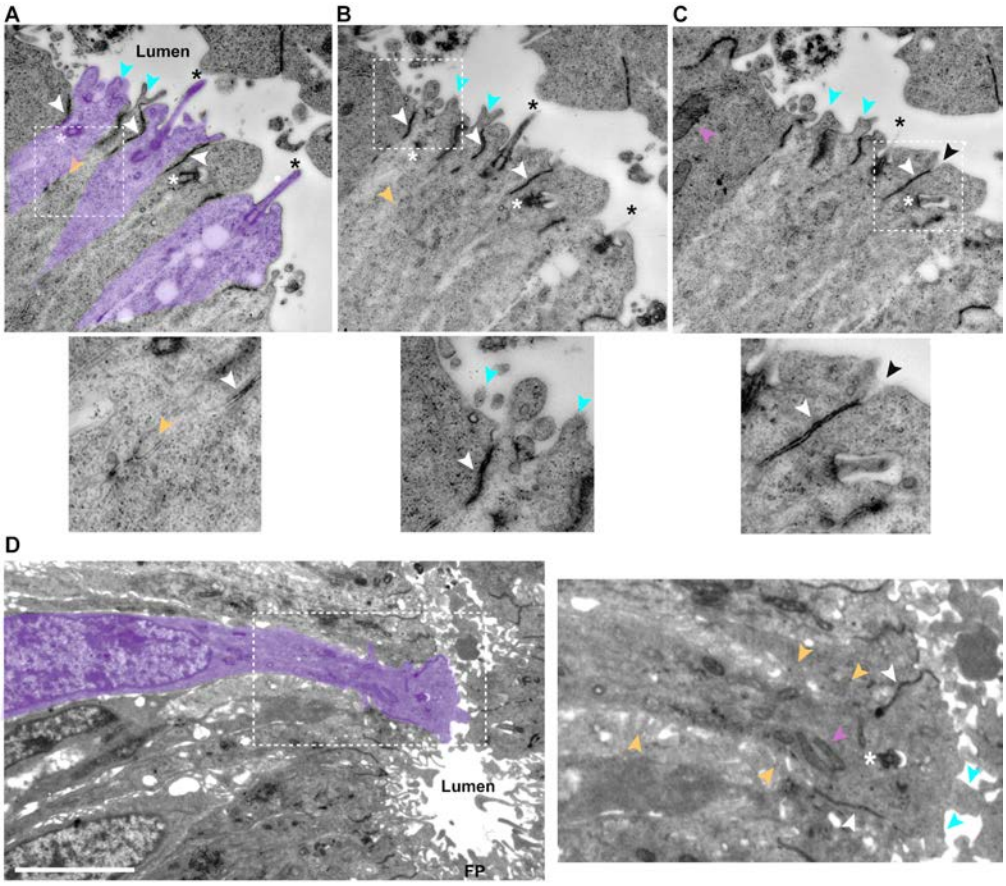

Figure 1 Ultra-structure of chicken and human embryo neuroepithelial apical endfeet
Serial transverse sections of chicken embryonic spinal cord (A-C), in A alternate endfeet are indicated in purple (excluding adherens junctions), white dashed line box is enlarged below each figure; (D)Transverse section though human embryonic spinal cord (CS12) in ventral region, including floorplate (FP), white dashed line box is enlarged in adjacent figure. Primary cilia tips in the lumen, black asterisks, and their basal bodies, white asterisks; adherens junctions (identified by electron dense material near abutting membranes), white arrowheads; microvilli, blue arrowheads; lateral protrusions, yellow arrowheads; mitochondria, pink arrowheads. Scale bar in D, 5 µm.

137 To investigate the dynamics of protrusive structures in apical endfeet, the neural tube of HH10-
138 12 chick embryos was transfected with a plasmid encoding the membrane marker pm-eGFP and
139 embryos cultured in ovo to stages HH17-18. This approach labelled cells in a mosaic fashion and allowed
140 rapid live imaging of individual endfeet membrane dynamics from the apical surface (enface) and up to
141 5 µm basally into tissue explants.

142 A variety of apical membrane protrusions were observed, and these could be classified based
143 on apico-basal position, size and dynamics. At the apical-most (lumen facing) surface short microvilli
144 (aka micro-spikes) (0.66 ± 0.21 µm) (Shepard et al., 1997, 1993) consistent with those identified by TEM
145 were most apparent, along with novel lamellipodia-like protrusive structures (1.44 ± 0.60 µm) which
146 may correspond to the thin plasma membrane found between endfeet by TEM; microspikes and these
147 apical lamellipodia-like protrusions (hereafter referred to as lamellopdia) were found in both live and
148 fixed tissue (Figures 2A,B). Monitoring F-tractin localisation further confirmed that both the lamellipodia
149 and the microvilli protrusions into the ventricle were actin rich (Movies 1-3). In addition, longer thin
150 protrusions (5.34 ± 1.89 µm) that extended into the lumen and across neighbouring endfeet were
151 observed at this apical-most surface. These filopodial-like protrusions were not apparent in our TEM
152 analysis, but have been reported previously in SEM analyses (Shepard et al., 1997, 1993). Strikingly,
153 these structures uniquely exhibited retrograde membrane movements (20-90 nm/s^{-1}), consistent with
154 the possibility of protein trafficking from the luminal space (Figures 2C-D, Movie 4).

155 Using this live imaging approach, a further set of membrane protrusions were observed, this
156 time emerging sub-apically, beneath the N-cadherin expressing adherens junction (Figure 2E, Movie 5)
157 and elongating lateral to the apico-basal axis, (Figure 2F, movie 6). These confirmed our EM observation
158 of sub-apical lateral protrusions: these are similar to protrusive structures recently described in the
159 developing mouse cortex (Shinoda et al 2018). In conclusion, the developing chick neuroepithelium
160 contains at least three types of dynamic apical membrane protrusions, (microvilli, lamellipodia and
161 filipodia), in addition to primary cilia, and exhibits sub-apical laterally extending protrusions, which
162 hereafter we will refer to as lateral protrusions (Figure 2G).
163

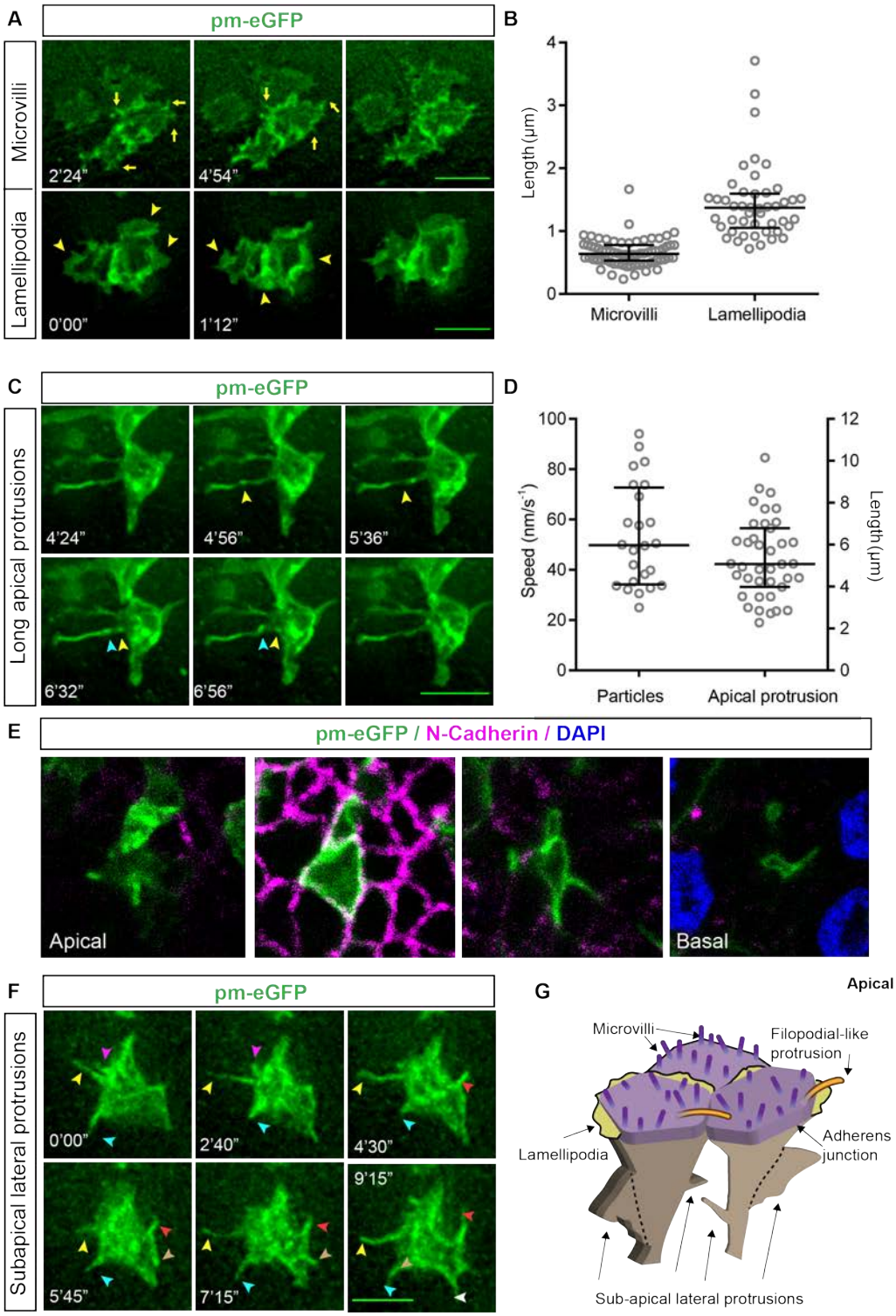

Figure 2 Live imaging analysis of apical and sub-apical protrusions extending from neuroepithelial apical endfeet
Enface live imaging of neuroepithelial cell apical end feet expressing the membrane marker pm-eGFP: (A) timepoints showing apical microvilli (yellow arrows) and lamellipodia (yellow arrowheads) at the apical surface; (B) quantification of microvilli and lamellipodial length (microvilli: 3 experiments, 7 explants, 28 cells, 70 microvilli; lamellipodia: 3 experiments, 7 explants, 46 cells); (C) long thin apical protrusions/ filopodia extending into the neural tube lumen, timepoints (and see movie 4); (D) quantification of surface protrusion length and speed of particle movement along the long thin apical protrusions (9 experiments, 14 explants, 39 cells); (E)Serial z stack images (apical to basal = right to left), showing sub-apical lateral protrusions emerging below N-cadherin expressing adherens junctions (pink); (F) timepoints showing sub-apical lateral protrusions, coloured arrowheads follow the dynamics of sub-apical protrusions over time; (G) Summary schematic of apical end foot protrusions, microvilli/microspikes, lamellipodia and long protrusions form at the apical surface (note primary cilia are not represented here). Sub-apical lateral protrusions emerge below the adherens junctions. Error bars in (B) and (D) are median with interquartile range. Scale bars in A, C, E, 5 µm.

Characterisation of a dynamic lateral protrusions within developing neuroepithelium

To characterise lateral protrusions, we mis-expressed pm-eGFP alone or together with pm-mKate2 and live imaged these structures at short intervals to capture their dimensions (thickness and length) as well as speed and direction of movement.

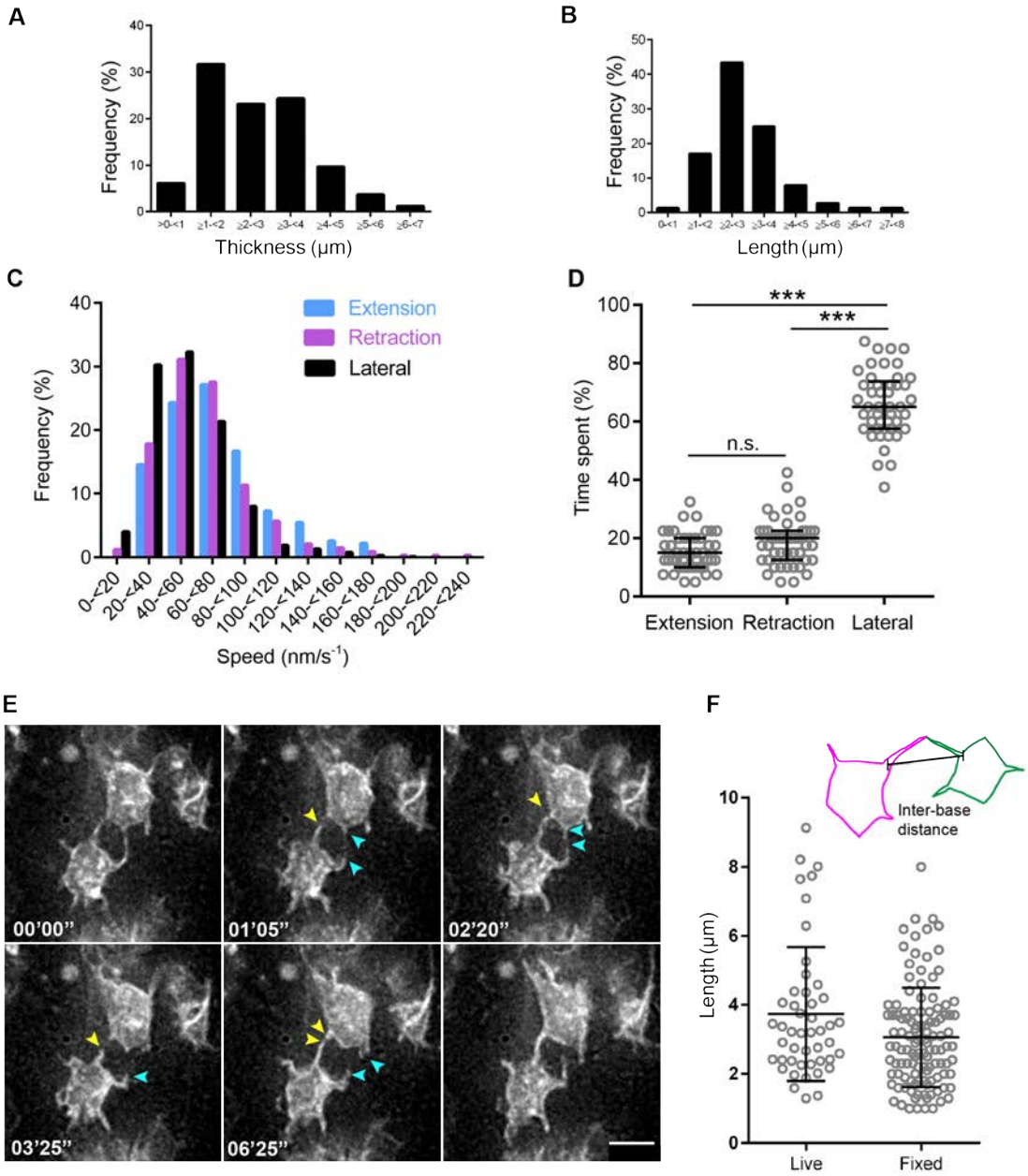

Figure 3 Characterisation of lateral protrusions

(A) Thickness of lateral protrusions and their frequency (3 experiments, 5 explants ,82 cells); (B) Protrusion length in contacting pairs (5 experiments, 9 explants, 48 pairs); (C) histogram of protrusion speed and frequency of extension, retraction, and lateral movement; (D) quantification of time individual protrusions extend, retract, or undergo lateral movement, total time analysed per protrusion is 10 minutes. One-way ANOVA test (Tukey's multiple comparisons test), n.s.= not significant, p= 0.1786; *** p <0.0001); (E) timepoints from live imaging of lateral protrusions. Arrowheads follow the dynamics of protrusions over time and cells express the membrane marker pm-eGFP; (F) quantification of lateral protrusion distance from their base, measured in fixed and live-imaged tissue (Fixed: 3 experiments, 7 explants, 116 cells; Live: 5 experiments, 9 explants ,47 cells), lines represent mean with SD. Error bar in (B) is median with interquartile range, and (D) is mean with SD. Scale bar in (E) 5 µm.

192 Measurement of individual lateral protrusions revealed these to be thick (2-4 µm), short
193 processes (most 2-3 µm, ranging up to 7 µm) (Figures 3A, B). To visualise lateral protrusion shape,
194 explants fixed at the end of live imaging sessions were subject to higher magnification imaging using
195 confocal microscopy to generate 3D models of apical end feet: these confirmed protrusion apico-basal
196 position, thickness and length (Figures 3A, B and Movie 7). The direction of lateral protrusion movement
197 was categorised as extension, retraction or lateral. Extension and retraction speeds ranged between 40-
198 80 nm/s^{-1} with a few more rapid examples at 160-180 nm/s^{-1} (Figure 3C). In contrast, lateral movement
199 was slower (20-60 nm/s^{-1}) and detected most of the time (Figure 3D): this may reflect passive
200 displacement influenced by shape change of neighbouring cells within the tissue.
201 A striking feature of lateral protrusions, made apparent by the mosaic transfection of cells, is
202 their extension around immediate neighbouring endfeet and contact with similar protrusions from
203 more distant cells within the tissue (Figure 3E, Movies 8 - 9). We measured the direct distance between
204 the base of protrusions that contact each other and found that the majority were 1-5µm apart, while a
205 subset reached across 5-10µm; similar findings were made in fixed tissue (live: 3.73 ± 0.28 µm, fixed:
206 3.1 ± 0.13 µm) (Figure 3F). As apical endfeet range from ~ 3-6 µm in diameter (Supplementary figure
207 1A) and lateral protrusions extend ~2-3 µm (Figure 3B), this indicates that most lateral protrusions make
208 contact with protrusions from non-neighbouring cells. The extent of protrusion-protrusion contacts
209 between non-neighbouring cells was next measured by analysing image Z-stacks. Most protrusion
210 contacts ranged up to 2 µm (Supplementary Figure 1 B).
211

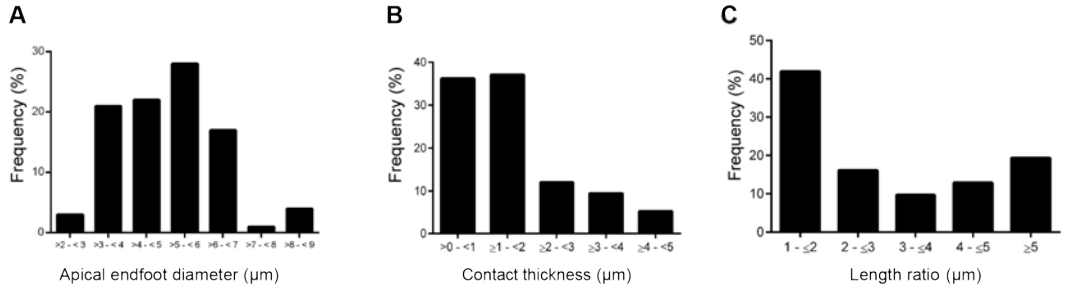

212
213
214 Supplementary Figure 1 Apical endfoot and lateral protrusion contact dimensions
215 (A) Range of apical endfoot diameters, most are between 3 and 6 µm (5 experiments, 9 explants, 98 cells); (B) Contact
216 protrusion thickness between non-neighbouring cells. In more than 70% of protrusion pairs, the contacting thickness did not
217 exceed 2 µm (4 experiments, 7 explants, 116 protrusion pairs); (C) Length ratio between contacting protrusions and their
218 frequency (4 experiments, 8 explants, 31 protrusion pairs).
219
220 In addition, it was clear that lateral protrusion length varied from cell to cell in contacting pairs
221 (Supplementary Figure 1C). Importantly, these protrusion-protrusion contacts were dynamic and could
222 persist for more than 10 minutes (longest contact time recorded 22’55’’) (Figure 4A). To investigate
223 contact dynamics in detail we transfected the neuroepithelium with a mixture of membrane markers
224 pm-eGFP and pm-mKate2 (Figure 4B), generating a mosaic of cells expressing either one of these

fluorophore-tagged proteins. Live imaging confirmed lateral protrusion extension around the curvature of neighbouring endfeet (Figure 4C and Movie 10) and revealed that protrusions from non-neighbouring cells meet tip to tip, extend along each other and also retract (Figures 4D – E, Movies 11 – 12). These behaviours suggest that lateral protrusions do not fuse but rather generate close membrane contacts between non-neighbouring cells.

Together these observations identify a new form of cell-cell contact within the developing neuroepithelium mediated by a sub-apical latticework of laterally extending protrusions, which connect non-neighbouring cells within 1-2 endfoot diameters.

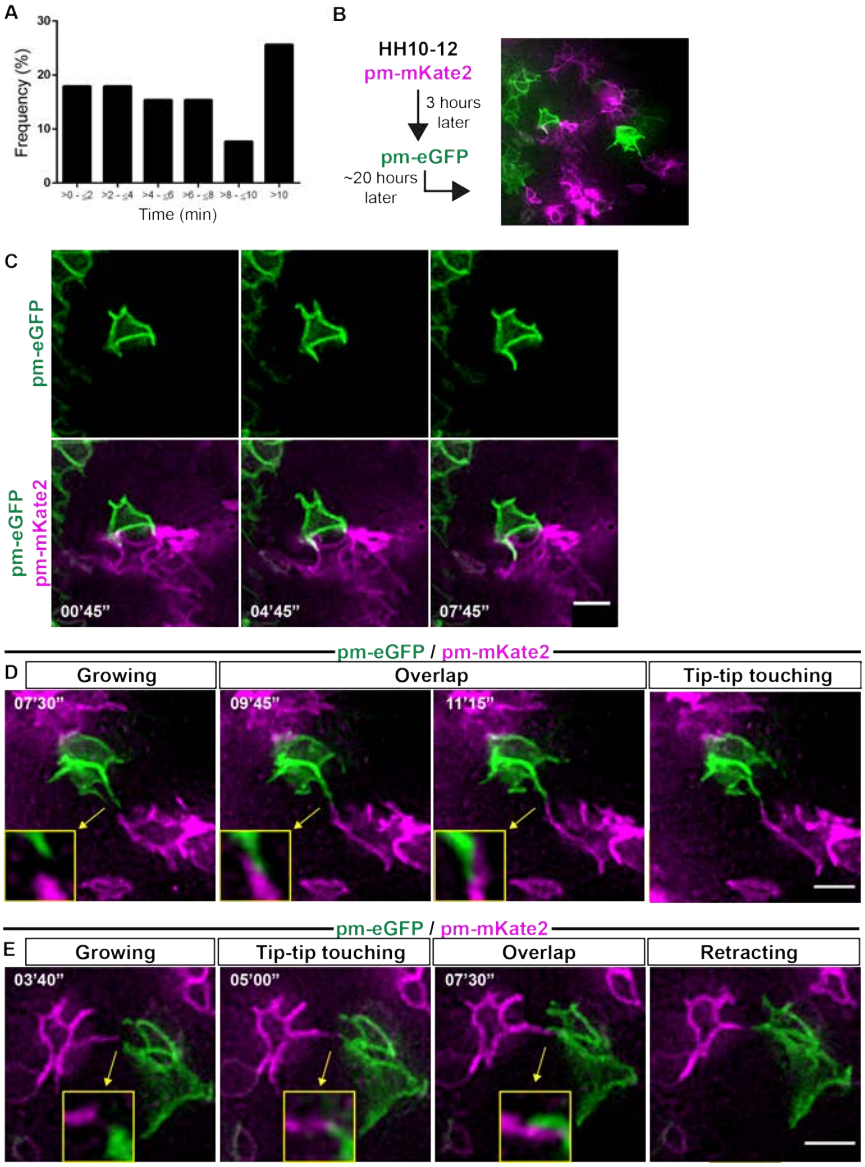

Figure 4 Lateral protrusion contacts from non-neighbouring cells extend along each other and can be long-lived
(A) Bar chart showing duration and frequency of protrusion contacts (5 experiments, 9 explants, 39 cell pairs); (B) strategy for generating mosaic pattern of pm-eGFP -pm-mKate2 pattern: cells are first transfected with pm-mKate2 at stage 10-12 and three hours later with pm-EGFP. Embryos are then left to develop to stage HH17-18 for live imaging; (C) timepoints showing that protrusions grow along the sides/edges of neighbouring cells; (D-E) timepoints showing protrusions from non-neighbouring cells contacting each other at their tips and extending along each other. Arrows and inset show the region magnified. Scale bars (C-E) 5 µm.

242 Unique cytoskeletal architecture distinguishes lateral protrusions

243 To characterise the cytoskeletal architecture of lateral protrusions, plasmids expressing constructs that
244 labelled actin (F-tractin-mKate2) or microtubule comets (EB3-sfGFP) were transfected along with
245 membrane markers into the neural tube. F-tractin-mKate2 localisation followed the extension and
246 retraction dynamics of the protrusions and was detected close to the protrusion tip (Figure 5A and
247 Movie 13). EB3-sfGFP comets showed a unidirectional movement from base to tip in most protrusions
248 (Figure 5B, Supplementary Figure 2A and Movie 14). Moreover, co-transfection of F-tractin-mKate2 and
249 EB3-sfGFP showed that actin and microtubules elongate to the same extent within lateral protrusions
250 (Supplementary Figure 2B-C).

251 Proteins involved in actin filament elongation in many different contexts include ENA and
252 vasodilator stimulated phosphoprotein (VASP) (Dent et al., 2007; Gallop, 2020; Kwiatkowski et al., 2007;
253 Lebrand et al., 2004). Ena/VASP are also proposed to support junctional actin assembly in tissue that is
254 under frequent tension of myosin-induced contractility, including at the level of adherens junctions
255 (Leerberg et al., 2014). To investigate if these proteins are localised to lateral protrusions, we mis-
256 expressed (as above) mNeonGreen-ENA or mNeonGreen-VASP together with the actin marker F-tractin-
257 mKate2 and both proteins were found at adherens junctions (Supplementary Figure 2D-E and Movies
258 15-16), and at lateral protrusion tips (Figure 5C, Movies 17 – 18). In contrast, a further tip localised
259 regulator of filopodial elongation, unconventional Myosin X (MYO10), e.g. (Sanders et al., 2013), was
260 detected uniformly in the cell cytoplasm but did not localise to lateral protrusion tips (Supplementary
261 Figure 2F). However, following mis-expression Myosin X was found at the tip of a separate set of longer
262 dynamics protrusions, the origin of which was difficult to determine (Movie 19). Along with their shorter
263 and broader dimensions, these further findings distinguish lateral protrusions from elongating filopodia,
264 which exhibit prominent tip localised Myosin X, and, consistent with their expression of Ena/VASP
265 (Damiano-Guercio et al., 2020) indicate that lateral protrusions have lamellipodia-like characteristics.
266
267
268
269

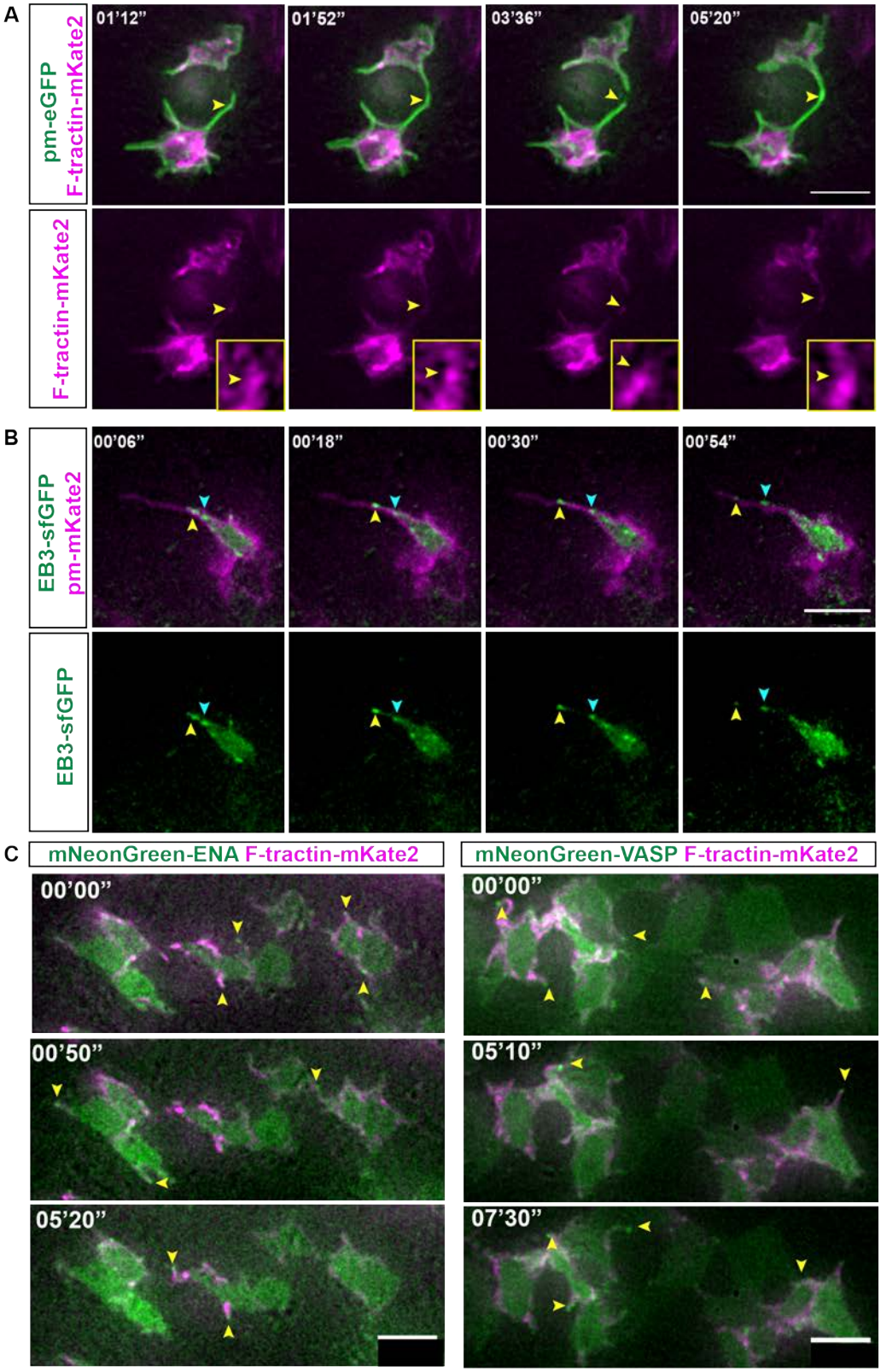

Figure 5 Actin, microtubules and ENA/VASP proteins localize to lateral protrusions

(A-C) Timepoints from live imaging sessions. (A) F-tractin-mKate2 follows the dynamics of membrane protrusions. Yellow arrowhead follows the F-tractin-mKate2 dynamics (2 experiments, 6 explants). Insets are of the region where the arrowhead is pointing. (B) Unidirectional microtubule movement from the base to the tip of the protrusion. Arrowheads follow the movement of EB3-sfGFP comets (2 experiments, 5 explants) (C) ENA and VASP localizing at the tip of protrusions (yellow arrowheads) (3 experiments, 10 explants). Scale bars (A-C) 5 µm.

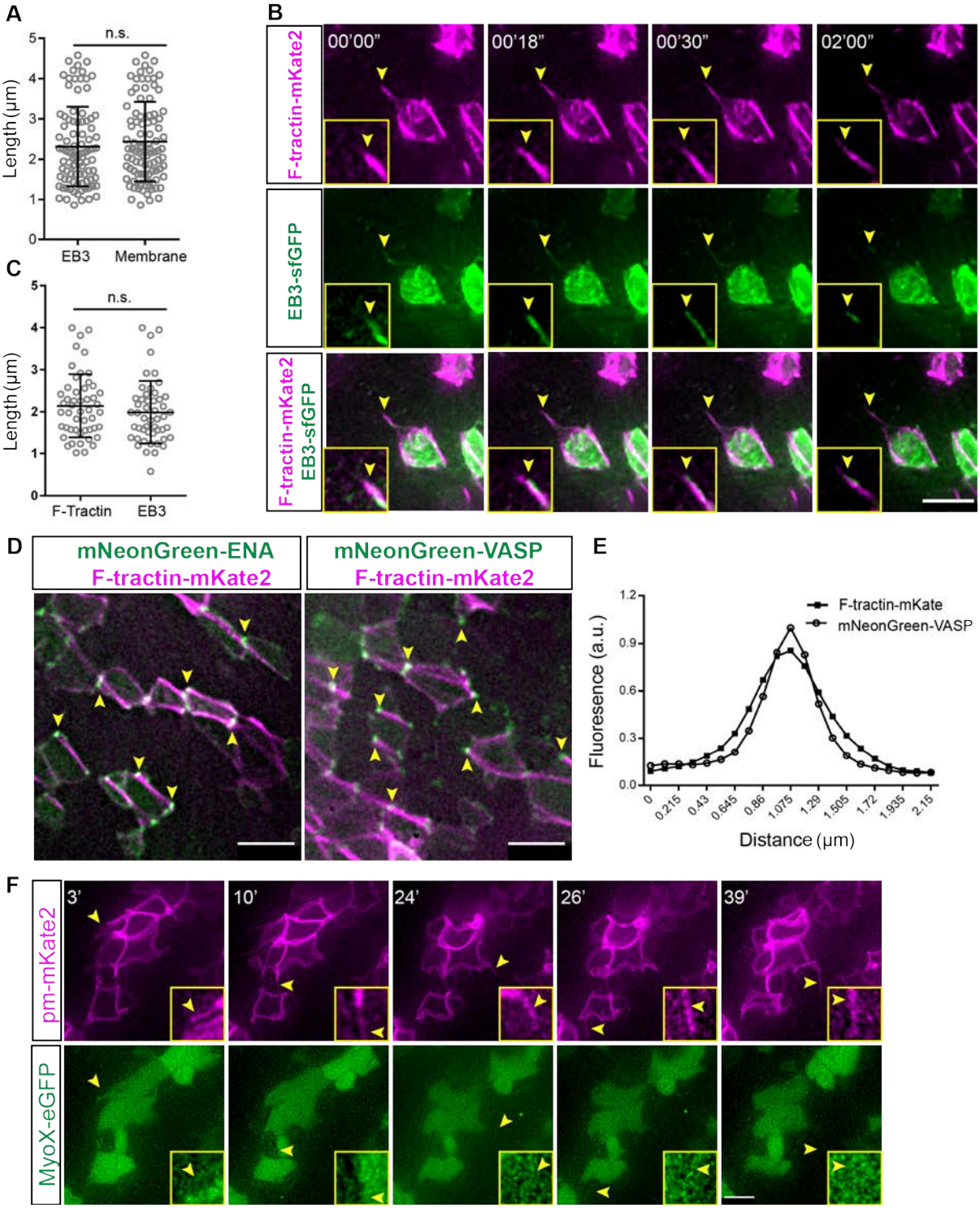

Supplementary Figure 2 Lateral protrusions cytoskeletal architecture

(A) Dot plot for maximal length travelled by EB-sfGFP comets in protrusions and the length of lateral protrusions using the membrane marker pm-mKate2 (2 experiments, 5 explants, 93 protrusions; t-test, n.s.= not significant, p = 0.3990); (B) Live imaging timepoints following mis-expression of EB-sfGFP and pm-mKate2, arrowheads and image insets show membrane protrusion tip and EB-sfGFP localization; (C) Dot plot for maximal length travelled by EB-sfGFP comets and the length of F-tractin-mKate2 in the same protrusions (2 experiments, 6 explants, 50 protrusions; t test, n.s. = not significant, p = 0.3104); (D) Live imaging timepoints following mis-expression of mNeonGreen-ENA or mNeonGreen-VASP with F-tractin-mKate2. At the level of adherens junctions, both mNeonGreen-ENA or mNeonGreen localized at cell junctions (yellow arrowheads); (E) Line graph showing fluorescence intensity of mNeonGreen-VASP and F-tractin-mKate2 at the cell junctions (2 experiments, 5 explants, 50 measurements); (F) Live imaging timepoints for MyoX-eGFP and pm-mKate2. MyoX-eGFP was detected in cytoplasm but did not localize to lateral protrusions (arrowheads). (A, C) Mean with standard deviation. Scale bars (B, D, F) 5 µm.

To monitor lateral protrusion dynamics over a longer period we next increased the imaging interval, which reduces photobleaching and potential photo-toxic effects: images were captured once a minute for one hour. This regime revealed the emergence of thin filopodia from the lateral protrusions (Figure 6A and Movies 20 – 21). These lateral filopodia had a homogenous thickness and were extended on average 5 times per hour (Figure 6B-C). Lateral filopodia were longer than the lateral protrusions themselves and the combined length of protrusions and filopodia averaged 4.7µm (Figure 6D) and so together can extend within the neuroepithelium beyond their immediate cell neighbours. Together these findings show that both actin and microtubules extend within these lateral protrusions, that these structures have lamellipodia-like characteristics and that emerging filipodia extend the reach of lateral protrusions.

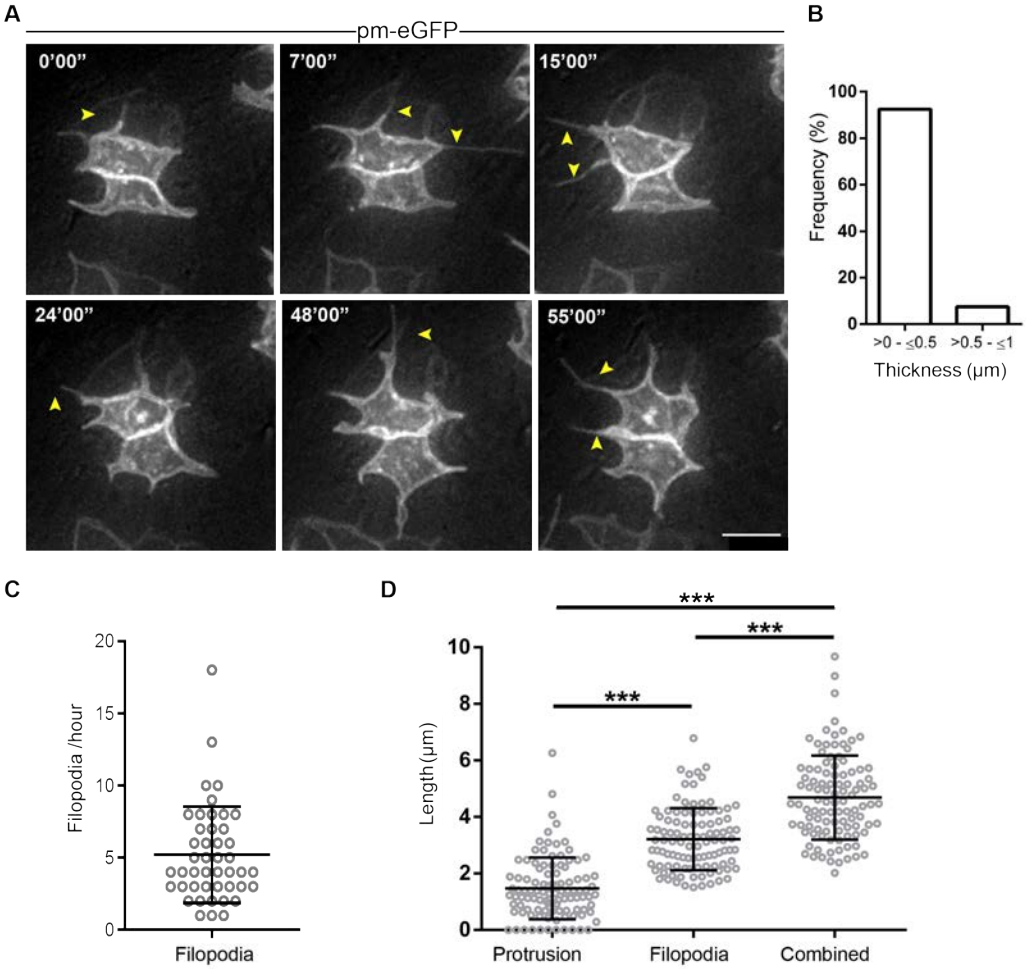

Figure 6 Filopodia emerge from lateral protrusions

(A) Live imaging timepoints showing presence of thin filopodial extensions (yellow arrowheads) emerging from lateral protrusions; (B) Bar chart showing filopodial protrusions are ~< 0.5µm in thickness (3 experiments, 5 explants, 65 filopodia); (C) Dot plot showing number of filopodia in one hour (5.2 ± 3.3 / hour) (4 experiments, 7 explants, 45 cells); (D) Filopodia are significantly longer than lateral protrusions, and combined filopodial-protrusion length extends lateral reach, (3 experiments, 5 explants, 27 cells) One-way ANOVA test (Tukey's multiple comparisons test), ***p<0.0001. (C, D) Mean with standard deviation. Scale bar (A) 5 µm.

313 Developing neuroepithelial cells do not share mitochondria via lateral protrusions

314 To investigate whether lateral protrusions act as tunnelling nanotubes within the neuroepithelium, we
315 mis-expressed the mitochondrial marker mNeonGreen-TOMM20 and the membrane marker pm-
316 mKate2. We then employed a fast imaging protocol to track both mitochondrial movements and cell
317 membrane dynamics. Despite the dynamic nature of mitochondria within the cell cytoplasm, transfer
318 between cells was never observed (Supplementary Figure 3A - B, Movie 22). We further generated and
319 analysed electron microscopy images of the apical neuroepithelium of developing chick and human
320 spinal cord for mitochondria localisation. These organelles were found in the apical endfoot in both
321 species but were not located in lateral protrusions and appeared too large to enter these structures
322 (Supplementary Figure 3 C- D). These live imaging and EM data, together with the finding that lateral
323 protrusions from non-adjacent cells extend along each other (Figures 4D, E) suggest that the meeting
324 of lateral protrusions does not lead to formation of cytoplasmic connection between cells.
325

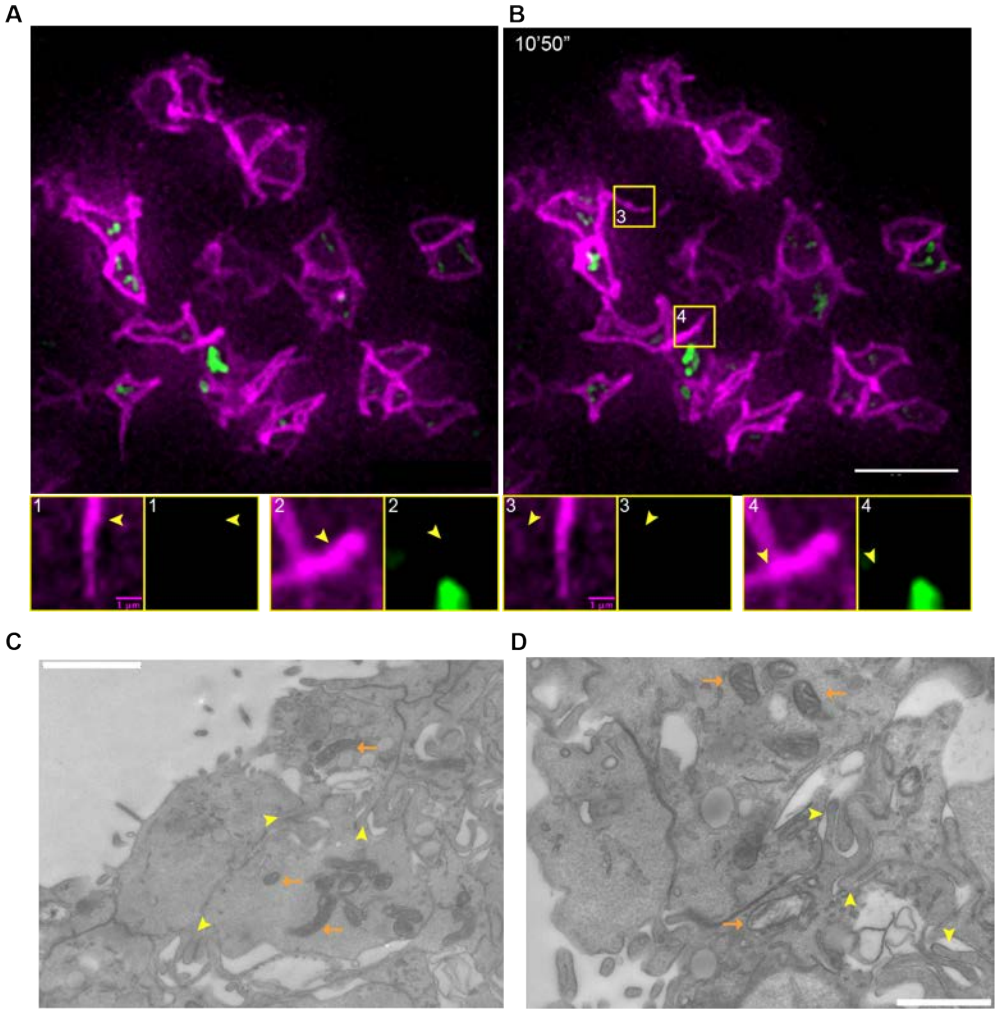

326
327
328 Supplementary Figure 3 Mitochondria do not enter lateral protrusions
329 (A, B) Live imaging timepoints (movie 22) following mis-expression of pm-mKate2 and the mitochondrial marker mNeonGreen-
330 TOMM20. Boxed regions of lateral protrusions are enlarged below, arrowheads indicate lateral protrusions (3 experiments, 9
331 explants); (C, D) enface EM sections from the apical surface of chick embryonic spinal cord at HH17-18 (sampled in 2 embryos),
332 showing lateral protrusions (yellow arrowheads) and mitochondria (orange arrows). Scale bars (A, B) 10 µm, (C, D) 1 µm.

333 Lateral protrusions depend on actin but not microtubule dynamics and lateral filipodia are also actin
334 dependent
335
336 To address whether actin or microtubule dynamics are necessary for the formation of lateral protrusions
337 the membrane marker pm-eGFP was introduced into the neuroepithelium (as above) and explants were
338 incubated in media containing Latrunculin-A (1µM), Taxol (10 µM) or control vehicle DMSO for one
339 hour, followed by live imaging. Latrunculin-A binds to free actin dimers and depletes the pool of
340 available actin for filament formation and maintenance, resulting in actin filament depolymerisation
341 over time (Coué et al., 1987). Taxol binds bundles and stabilises microtubules, perturbing
342 depolymerisation events (Schiff and Horwitz, 1980). Exposure to Latrunculin-A reduced lateral
343 protrusion dynamics and lead to quantifiable inhibition of lateral filopodia formation, while Taxol had
344 no effect on these structures (Figures 7A, B, movies 23 – 25). These data show that lateral protrusions
345 and filopodia rely on actin but not microtubule dynamics for their extension.
346
347 Lateral protrusions rely on the actin binding protein WAVE1
348 To monitor and manipulate actin dynamics on a cell-by-cell basis and more specifically in lateral
349 protrusions we looked for an actin regulatory protein that might act in these structures. Branched actin
350 filament networks are assembled through the combined activities of the Arp2/3 complex and different
351 forms of WASP/WAVE proteins. In *Drosophila*, loss of SCAR/WAVE1 complex activity in notum
352 epithelium results in specific loss of basolateral protrusions (Georgiou and Baum, 2010). TIRF imaging
353 has also shown that in comparison with WAVE2 and N-WASP, WAVE1 generates shorter, slower growing
354 actin filaments (Miki et al., 1998; Sweeney et al., 2015; Yamazaki et al., 2005), consistent with the form
355 and dynamics of lateral protrusions we observe here. Moreover, mutations in human WASF1/WAVE1
356 Arp2/3/actin binding domain led to inhibition of fibroblast lamellipodial protrusion (Ito et al., 2018),
357 further identifying WAVE1 as a potential mediator of lateral protrusions. As this region is highly
358 conserved across species (Ito et al., 2018), we cloned and eGFP-tagged the full-length (FL) human
359 WAVE1 and a C-terminal truncated form of the protein (informed by the nonsense mutation described
360 by Ito et al (Figure 7C). This truncation generates a protein lacking the C and A domains and part of the
361 WH2 domain necessary for binding actin and the Arp2/3 complex to promote actin polymerization
362 (Boczkowska et al., 2014; Ito et al., 2018). We predicted that mis-expression of truncated (Δ) WAVE1-
363 eGFP would have a dominant negative action, competing with endogenous WAVE complex-binding
364 partners.
365 When mis-expressed at low levels, FL-WAVE1-eGFP or ΔWAVE1-eGFP localized at cell-cell
366 junctions and at the base of lateral protrusions (Figure 7D). When ΔWAVE1-eGFP was expressed, most
367 lateral protrusions were lost (some transient filopodia were observed, Movie 27) and the endfoot
368 acquired a round-ended appearance: in contrast, this phenotype was only occasionally observed

following high level WAVE1-eGFP mis-expression (Figures 7E, F, movies 26, 27). These data show that apical endfoot shape and lateral protrusion dynamics rely on WAVE1 and moreover, indicate that mis-expression of the ΔWAVE1 can be used to interfere with lateral protrusion formation on a cell-by-cell basis.

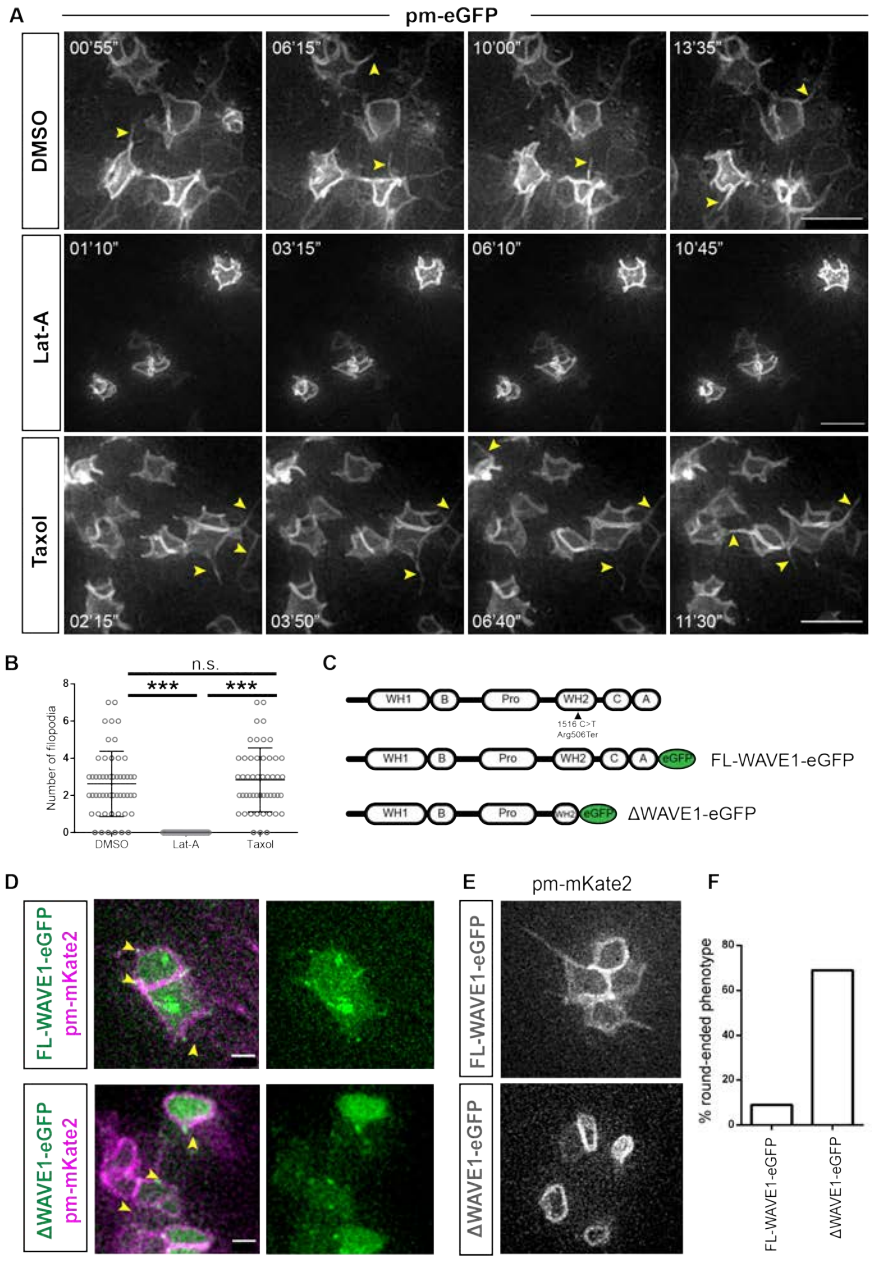

Figure 7 Lateral protrusion dependence on Actin/WAVE1 and ΔWAVE1 round-ended apical endfoot phenotype
(A) Live imaging timepoints monitoring lateral protrusions and filopodia in the presence of DMSO control, Latrunculin-A (Lat A) or Taxol; (B) quantification of filopodial protrusions in each condition in A, Lat A inhibits filapodial extensions compared to DMSO control and Taxol treatments, One-way ANOVA test (Tukey's multiple comparisons test), p= 0.3852; ***p<0.0001.), error bars = mean with SD; DMSO: 3 experiments, 6 explants, 44 cells; Latrunculin-A: 3 experiments, 9 explants, 337 cells; Taxol: 2 experiments, 5 explants, 50 cells; (C) Schematic of domain composition of the human WAVE1/WASF1 protein and the nonsense mutation (Arg506Ter) identified in (Ito et al., 2018), and details of constructs used for experiments: full length (FL-WAVE1) and truncated protein (ΔWAVE1) with C-terminus eGFP tag; (D) Low-level mis-expression of FL-WAVE1-eGFP and ΔWAVE1-eGFP both localised in cell membrane at the base of lateral protrusions; (E) Round-ended apical endfoot phenotype in cells mis-expressing ΔWAVE1-eGFP, but not FL-WAVE1-eGFP, images extracted from movies 26 and 27; (F) percentage of cells with round-ended phenotype following FL-WAVE1-eGFP and ΔWAVE1-eGFP mis-expressions. FL-WAVE1-eGFP: 12/133 [9%], 4 experiments, 8 slices, 133 cells and ΔWAVE1-eGFP: 116/167 [69%], 2 experiments, 4 slices, 167 cells. Scale bars in (A) 5 µm and in (D) 2 µm.

387 Loss of lateral protrusions does not alter expression of adherens junction protein N-cadherin nor disrupt
388 neuroepithelial tissue integrity
389
390 To address the functional significance of lateral protrusions, we first investigated whether their loss
391 affected maintenance of adjacent adherens junctions (AJ). Adherens junction constituent protein N-
392 Cadherin localisation appeared unaltered at the apical surface across the dorsoventral axis of the neural
393 tube following ΔWASF1-eGFP mis-expression, suggesting that AJs remain intact, despite the loss of
394 lateral protrusions (Figure 8A). The developing, neuron-generating, neuroepithelium lacks tight
395 junctions which are initially located subapically, below the adherens junction (Aaku-Saraste et al., 1996).
396 This raised the possibility that sub-apical protrusions facilitate neuroepithelial integrity. To test this
397 70kDa TxRd-Dextran was injected into the neural tube lumen and dextran leakage into the
398 neuroepithelium in the presence of ΔWASF1-eGFP or control pm-eGFP was assessed; however, no
399 differences were apparent after 24h Supplementary Figure 4). These data indicate that within this
400 developmental window loss of lateral protrusions does not alter AJs between cells nor impact
401 neuroepithelial tissue integrity.
402
403

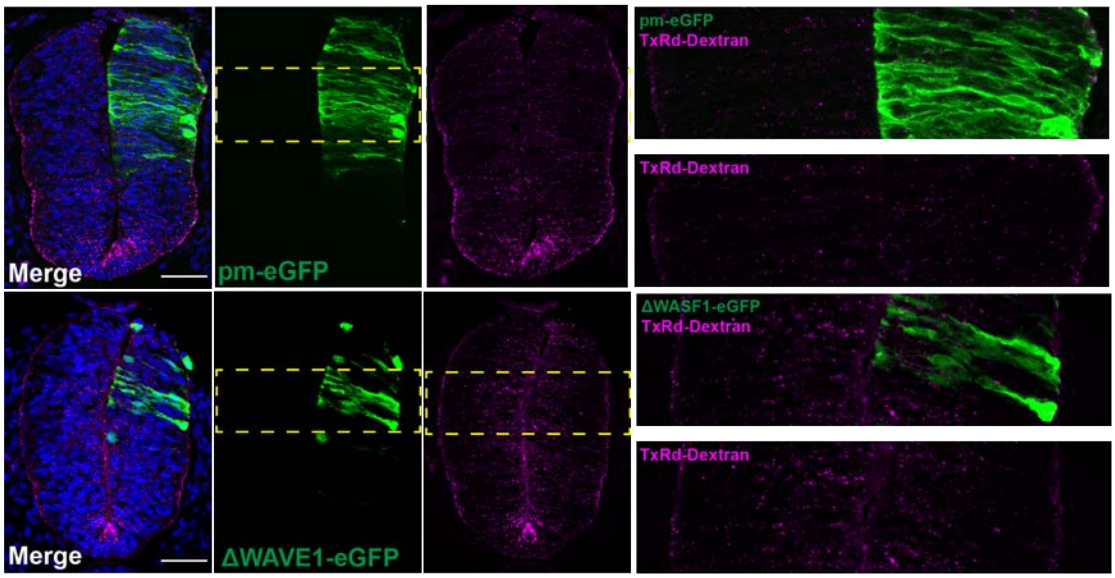

404
405
406 Supplementary Figure 4 ΔWAVE1-eGFP does not compromise apical neuroepithelial integrity
407 Transverse sections through HH17-18 neural tube following misexpression of control pm-eGFP or ΔWASF1-eGFP and
408 introduction of Texas Red-Dextran (70kDa) into the neural tube for 24h. No qualitative change in the levels of Texas Red-
409 Dextran between the two conditions was observed (pm-eGFP = 4 embryos, ΔWASF1-eGFP = 4 embryos). Scale bars 50 µm
410
411
412
413
414

415 **Neuronal differentiation involves withdrawal of lateral protrusions, but precocious loss of these**
416 **protrusions is insufficient to trigger neurogenesis**
417 Neuronal differentiation involves the delamination of newborn neurons, during which they are released
418 from apical connection with neighbouring cells (Itoh et al., 2013; Kasioulis and Storey, 2018; Rousso et
419 al., 2012; Zhang et al., 2010). This includes an abscission process which operates at the level of the AJs
420 (Das and Storey, 2014) and may also involve withdrawal of the lateral protrusions described here. To
421 investigate whether this latter step is involved in the regulation of neurogenesis, we first compared
422 protrusion characteristics in TuJ1 expressing newborn neurons (which have yet to delaminate) and
423 neural progenitors. To increase the number of newborn neurons we drove this process by mis-
424 expressing the proneural factor neurogenin2 (Neurog2-IRES-GFP) together with pm-eGFP in the neural
425 tube (as above). Protrusion dimensions were measured in fixed tissue enface following
426 immunofluorescent detection of TuJ-1 and N-Cadherin for AJs. TuJ-1 expressing newborn neurons had
427 a smaller apical endfoot area (measured at the level of the AJ) and exhibited significantly reduced lateral
428 protrusion thickness and length (Figures 8B -D, Movies 29 – 30). These data suggest that differentiating
429 neurons normally withdraw their lateral protrusions prior to delamination.
430 This finding raised the possibility that ΔWAVE1-eGFP expressing cells lacking lateral protrusions
431 might undergo precocious neuronal differentiation. To test this, ΔWAVE1-eGFP or control pm-eGFP
432 was mis-expressed in the neural tube and assessed after 48h. Cells expressing the neuronal marker
433 HuC/D were then quantified, however, the proportion of HuC/D expressing cells was unaltered between
434 electroporated and non-electroporated sides in ΔWAVE1-eGFP expressing as well as in control embryos
435 (Figures 8E – F). Furthermore, analysis of expression of newborn neuron marker, the Notch ligand Delta1
436 (Dll1) (Henrique et al., 1995), in ΔWASF1-eGFP transfected embryos also revealed no changes in
437 expression pattern at 24h (data not shown). Together, these findings suggest that while withdrawal of
438 lateral protrusions is regulated by the neuronal differentiation programme, this step alone is insufficient
439 to trigger this process.

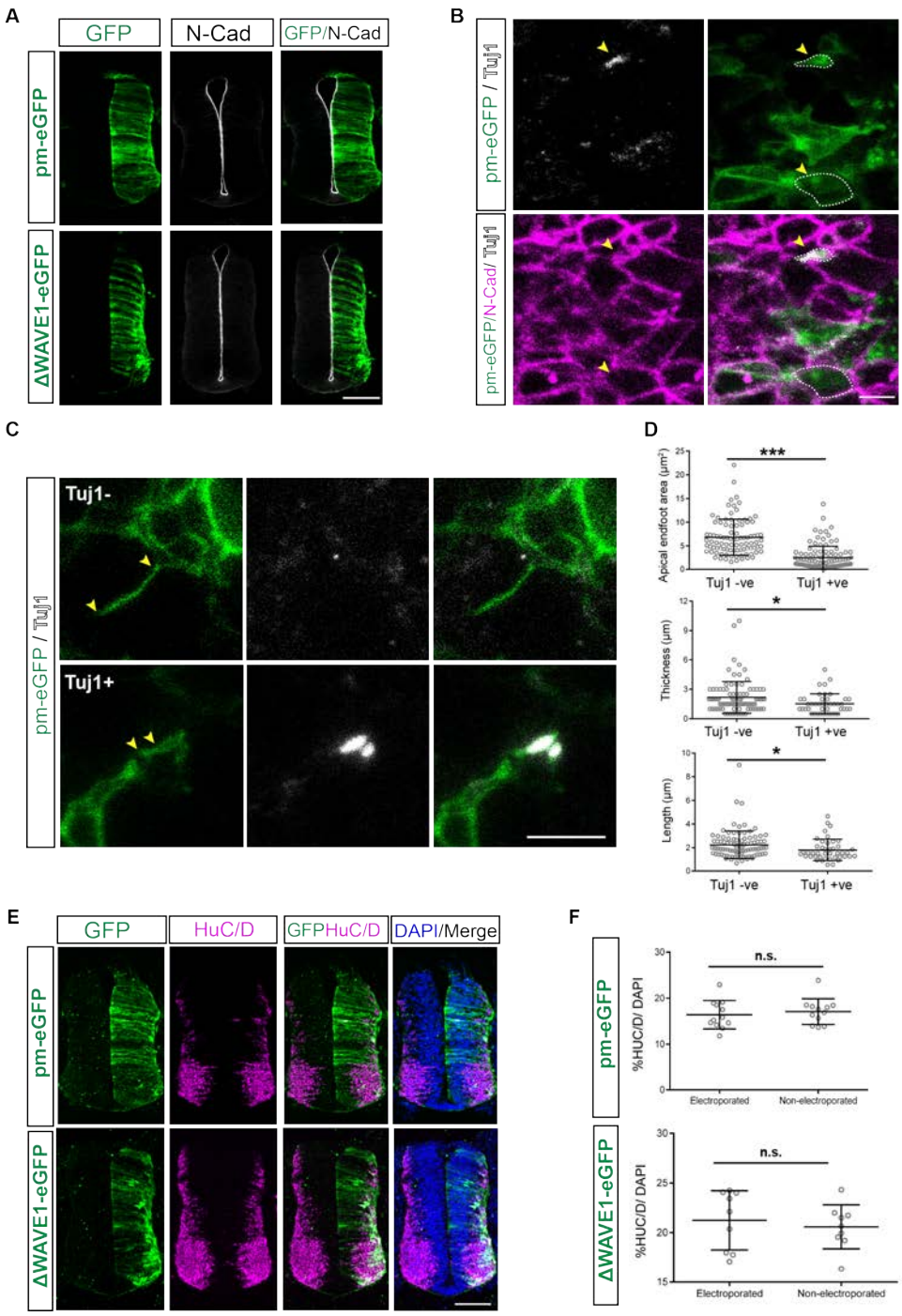

Figure 8 ΔWAVE1 mis-expression does not alter N-Cadherin expression and although neurogenesis involves lateral protrusion withdrawal, ΔWAVE1 does not trigger neurogenesis

(A) No alternation in AJ protein N-Cadherin following mis-expression of control pm-eGFP or ΔWAVE1-eGFP in neural tube for 48 hours (> 3 transverse sections from each of pm-eGFP = 4 embryos, ΔWASF1-eGFP = 4 embryos); (B) Tuj1+ and Tuj1- apical endfeet viewed enface at the level AJ/N-Cadherin expression (pink), white dashed lines examples of areas measured; (C) Lateral protrusion length measurement (between yellow arrowheads) in Tuj1+ and Tuj1- cells (see movies 28, 29); (D) Dot plots showing significant difference in apical endfoot area, and lateral protrusion thickness and length between Tuj1- and Tuj1+ cells (t-tests for area: 4 experiments, 10 explants, Tuj1+ cells = 103; Tuj1- cells = 93, p = 0.0001; thickness and length: 4 experiments, Tuj1+ cells = 43, Tuj1- cells = 93, thickness p = 0.0172, and length: p = 0.0335); (E) No alternation in numbers of neurons (HuC/D +ve cells) following mis-expression of control pm-eGFP or ΔWAVE1-eGFP in the neural tube for 48 hours, quantified in (F) percentage of HuC/D +ve cells on electroporated and non-electroporated sides of the neural tube (> 3 transverse sections from each of pm-eGFP = 3 embryos, ΔWASF1-eGFP = 4 embryos, t-test pm-eGFP p = 0.7496; ΔWASF1-eGFP, p = 0.4266). (C and E) Mean with standard deviation. Scale bars, A and E 100µm, C 5 µm.

455 Discussion

456 This study provides a comprehensive live view of cellular protrusions that extend from the apical
457 neuroepithelium and uncovers a sub-apical latticework of lateral protrusions and associated fine
458 filopodia which mediate membrane contacts between non-neighbouring cells within this tissue. The
459 presence of growing microtubules as well as actin in lateral protrusions, the localised expression of ENA
460 and VASP proteins and lack of atypical Myosin-10 in these structures, together with their lamellipodia-
461 like morphology, distinguished these structures from cytonemes. The absence of mitochondria, along
462 with the overlap rather than fusion between lateral protrusions from distant cells further discriminate
463 these structures from tunnelling nanotubes. Despite the presence of microtubules, lateral protrusions,
464 and their extending filopodia, were only dependent on actin polymerization. We further show that the
465 actin nucleating protein WAVE1 localises to lateral protrusions and that introduction of mutant WAVE1
466 leads to their loss. Importantly, this did not alter localisation of adherens junction protein N-cadherin
467 nor disrupt neuroepithelial tissue integrity. While lateral protrusions were specifically withdrawn prior
468 to delamination of newborn neurons, experimentally induced precocious loss of these structures was
469 insufficient to trigger neurogenesis. These findings suggest that lateral protrusion withdrawal is
470 regulated by the neuronal differentiation programme and that re-configuration of the actin/WAVE1
471 network is an early step that anticipates neuronal delamination. Overall, this study identifies a dynamic
472 sub-apical latticework of lateral protrusions which has the potential to mediate cell-cell communication
473 across the developing neuroepithelium.
474
475 Ultra-structure analyses and live imaging of the lumen facing apical membrane of
476 neuroepithelial cells revealed three distinct apically protrusive structures, in addition to the primary
477 cilium; microvilli (also known as micro-spikes), lamellopodia-like structures and long filopodia, all of
478 which could be further visualized with F-tractin and so are actin-based. The presence of microspikes on
479 neuroepithelial cells has been reported previously using electron microscopy to analyze the closing
480 neural tube in chicken and rodent embryos (Shepard et al., 1997, 1993; Smith et al., 1982; Waterman,
481 1976). Later work revealed localization of the surface glycoprotein prominin-1 (CD133) on
482 neuroepithelial cell microvilli (Marzesco et al., 2005), suggesting that these serve to increase the apical
483 surface area for internalization of potential growth factors present in the lumen. Most recently, in Caco-
484 2 intestinal epithelial cells, actin assembly has been shown to drive microspike protrusions toward apical
485 adherens junctions and increase the surface membrane available for Cadherin mediated cell-cell-
486 adhesion (Li et al., 2021, 2020) which might be conserved in the neuroepithelium. We further
487 document, to our knowledge, novel apical lamellipodial protrusions, the dimensions of which suggest
488 that they can reach over neighbouring apical endfeet and so may influence their neighbours and/or
489 operate to sense the immediate environment. Finally, we observed long apical filopodia that contact

490 non-neighbouring cells. Such protrusions have been noted previously in fixed tissue (Shepard et al.,
491 1997, 1993; Waterman, 1976). We reveal here that these apical filopodia exhibit retrograde membrane
492 movement indicative of active endocytosis of components from the environment. In support of this
493 possibility, signaling pathways such as sonic hedgehog and Wnt show the binding and trafficking of the
494 ligands along such cytoneme-like membrane protrusions in the chick limb mesenchyme (Sanders et al.,
495 2013) and early zebrafish neural plate (Stanganello et al., 2015).

496 The presence of lateral protrusive structures has been reported previously in a range of non-
497 neural epithelia (Demontis and Dahmann, 2007; Farquhar and Palade, 1965; Tang and Brieher, 2012).
498 Recent work in developing mouse cerebral cortex identified very similar lateral lamellipodia-like
499 structures by EM and reported their actin dependence (Shinoda et al., 2018). We confirm the sub-apical
500 emergence of lateral protrusions in the chicken and human spinal cord using EM. In the chick, live
501 imaging further revealed that these lamellipodia-like protrusions create contacts between non-
502 neighbouring cells and provide a platform for filopodial extensions, forming dynamic membrane
503 contacts with a radius of at least two apical endfeet (> ~5 microns) from each neuroepithelial cell:
504 effectively forming a latticework of cell contacts within the neuroepithelium. Our findings suggest that
505 these contacts do not involve cell fusion (they extend along each other and appear not to traffic
506 mitochondria) and so are distinct from tunnelling nanotubes (Korenkova et al., 2020; Rustom et al.,
507 2004). However, future studies could assess further potential trafficked organelles, including lysosomes
508 and endosomes.

509 The lamellipodial-like structure of lateral protrusions shares some similarity with basal
510 protrusions described in *Drosophila* notum epithelium (Georgiou and Baum, 2010). Importantly, these
511 basal protrusions are uniquely SCAR/WAVE dependent and consistent with this we found the related
512 branched actin nucleating protein WAVE1 (Carlier et al., 2015; Pollard and Borisy, 2003) was localised
513 to and required for lateral protrusions. Moreover, WAVE regulatory complexes work cooperatively with
514 Ena/VASP to enhance Arp2/3 mediated actin assembly in lamellipodia (Chen et al., 2014) and see
515 (Damiano-Guercio et al., 2020), and ENA and VASP localisation to lateral protrusion tips here further
516 identifies these as lamellipodia-like structures. However, it is important to note that WAVE1 also
517 localises to mitochondria in fibroblasts (Ito et al., 2018), and we observe this in neuroepithelial cells too,
518 so its regulation of lateral protrusions could also reflect an indirect WAVE1 function in this organelle.
519 Lateral protrusions were additionally distinguished by the presence of polymerising microtubules from
520 base to tip, while most cellular protrusions are exclusively composed of actin, or have microtubules
521 confined to the base (González-Méndez et al., 2019). Indeed, together these findings identify a
522 surprising similarity between sub-apical lateral protrusions and their extending filopodia and the
523 cytoskeletal organisation of later forming axonal growth cones (Robert Manak, 2018).

524 The discovery that lateral protrusions are withdrawn by newborn neurons that are still attached
525 at the apical surface suggests that this step is an early event directed by the neuronal differentiation
526 programme. Moreover, precocious reduction of lateral protrusions induced by mis-expression of a
527 mutant form of WAVE1 was insufficient to trigger neurogenesis. Importantly, neuronal delamination
528 and differentiation is elicited by loss of AJ constituent proteins N or E Cadherin (Hatakeyama et al., 2014;
529 Itoh et al., 2013; Rousso et al., 2012). It is therefore not surprising that reduction of WAVE1 and lateral
530 protrusive activity also did not impact N-Cadherin expression or localization. This is further consistent
531 with findings in the *Drosophila* notum epithelium, where loss of SCAR/WAVE1 complex activity similarly
532 does not impact apico-basal polarity (Georgiou and Baum, 2010). These findings suggest that regulation
533 of WAVE1 activity in lateral protrusions is an early action of the neuronal delamination mechanism and
534 supports the notion that this anticipates the extensive actin network re-configuration apparent during
535 apical abscission (Das and Storey, 2014; Kasioulis et al., 2017). The importance of actin configuration in
536 this process is further underlined by the requirement for the actin cross-linking protein Filamin A,
537 mutation of which underlies defective neuronal delamination in the human condition periventricular
538 heterotopia (Parrini et al., 2016; Sheen et al., 2001; Zhang et al., 2013).
539 Overall, our findings indicate that withdrawal of lateral protrusions is regulated by, but does not
540 drive, the neuronal differentiation programme and that these structures may be part of the mechanism
541 that apically anchors cells within the neuroepithelium. However, this does not exclude roles in cell
542 communication for this latticework of cell membrane contacts (Figure 9). One possibility is that lateral
543 protrusions, which radially contact cells several endfeet away, facilitate cell-cell coupling within cell
544 micro-clusters, which have recently been shown to exhibit synchronous Hes gene (Notch signalling)
545 oscillations, and so may serve to regulate neuron production (Biga et al., 2021). Indeed, a role in local
546 coordination of cell signalling is consistent with lateral protrusion withdrawal in newborn neurons,
547 which might then experience reduced signalling from neighbouring cells, while subsequently delivering
548 Notch ligand via adherens junctions (Hatakeyama et al., 2014), and see (Falo-Sanjuan and Bray, 2021).
549 This an interesting idea because it could provide a cell biological basis for the compartmentalization of
550 cell selection within the developing neuroepithelium. The lateral protrusion latticework also provides
551 an opportunity to relay signals across the developing neuroepithelium. Such relays may be required to
552 convey signalling beyond the reach of ligand diffusion in extracellular space/neural tube lumen and/or
553 delivery by cytonemes/long filopodia. The potential for lateral protrusions to facilitate comparison and
554 integration of signalling between cells in this further context suggests a role in establishing and/or
555 maintaining positional information across the neuroepithelium. To elucidate these functional roles,
556 future studies should assess local patterns of contact dynamics and localise ligands and receptors in
557 lateral protrusions.

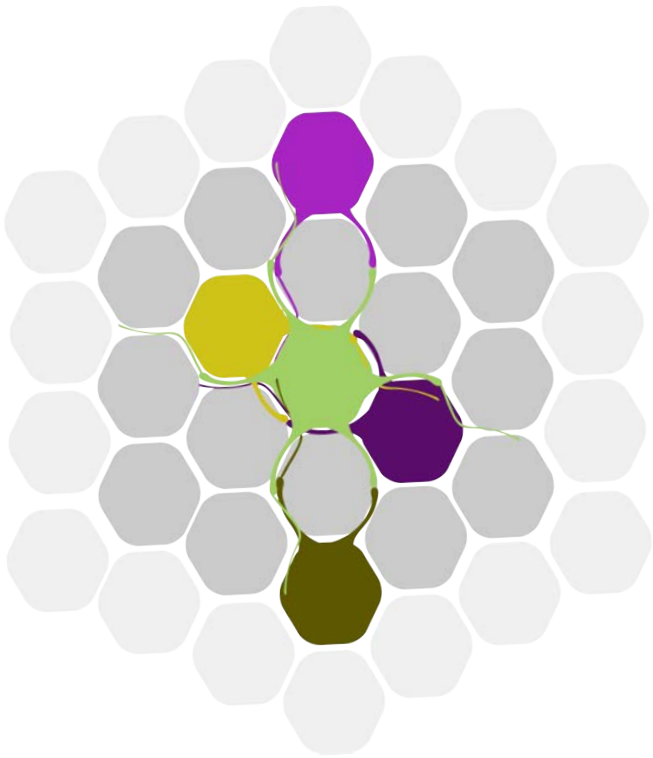

Figure 9 The lateral protrusion latticework

Schematic depicting exemplar interactions of lateral protrusions extending from one apical end foot (light green). Lateral protrusions with filipodia can make contacts with cells and their protrusions 1-2 endfeet away (light purple and dark green), while also experiencing mutual contacts with their immediate neighbours (yellow, dark purple). Lateral protrusions from non-neighbouring cells can meet and retract or extend along each other. As all apical endfeet extend lateral protrusions this creates a latticework of short-range cellular protrusions with the potential to mediate cell-cell communication across the neuroepithelium.

Acknowledgements

We are grateful to our colleagues Kees Weijer and Jens Januschke for comments on this manuscript, to Raman Das for preparation of chicken embryonic spinal cord for electron microscopy and imaging by John James presented in Figures 1A-C and to Professor Tim Sanders, (The Neuroscience Institute University of Chicago), for sharing plasmid constructs. Human embryonic tissue in this study was provided by a Joint MRC/Wellcome Trust grant (# MR/R006237/1) to the Human Developmental Biology Resource (www.hdbr.org). IK, AD and PH were supported by a Wellcome Investigator award to KGS (WT102817AIA). The confocal microscope used for imaging was purchased with support from a Wellcome Trust Multi-User Equipment grant (WT101468).

The authors declare that they have no conflict of interest.

580 Materials and Methods

581 Tissue sources

582 Fertilised Bovans Brown chicken eggs were supplied by Henry Stewart & Co. Ltd and incubated at 38 °C
583 to the desired Hamburger and Hamilton (HH) stage. Work with chicken embryos at the stages
584 investigated here do not require ethical approval. Fixed human embryonic spinal cord tissue at Carnegie
585 stage (CS)12 used for EM studies was provided by the Human Developmental Biology Resource (HDBR)
586 project # 200407.

587

588 Cloning

589 The ImProm-II reverse transcription system (Promega, A3800) was used to generate cDNA from hESC
590 (H9) RNA. Full length WAVE1 was PCR amplified adding in a linker sequence. The WAVE1 PCR product
591 was then used to amplify the mutant WAVE1 (ΔWAVE1), (a truncated version of the gene lacking
592 sequence distal to nonsense mutation Arg506Ter, Ito et al 2018, see Figure 6C) to which the linker
593 sequence was added in a second round of PCR. Both were tagged with monomeric eGFP, separated by
594 the linker sequence, in a further PRC reaction. For primers for full length WAVE1 (FL) and ΔWAVE1 see
595 Table 1. PCR reactions were carried out using the Phusion polymerase (ThermoFisher, F537). Following
596 each reaction, the products were gel extracted using the Zymoclean Gel DNA recovery kit
597 (D4001). The pENTR/D-TOPO cloning kit (ThermoFisher, K240020) was used to introduce the PCR
598 products into the entry vector for Gateway cloning. PCR products in the entry vector were then
599 recombined in the destination vector using the LR clonase II enzyme mix (ThermoFisher, 11791100). We
600 utilised the PBX destination vector (kind gift from Timothy Sanders (Sanders et al., 2013) which contains
601 the CAG promoter, for efficient expression in chicken tissue.

602

603 Table 1- Primer sequences

604

Primer	Sequence
WAVE1 Forward	CACCATGCCGCTAGTGAAAAGAAACATCGATCCTAGGCACTTGTGC
WAVE1 Reverse + Linker	GGAACCGCCACCACTCCCGCCACCGGACTCCAACCAATCTACTTCATCAAATTCTGAATCATC
ΔWAVE1 Reverse	TATTGCTTCCAGTAGCACACTCCTGGCATCACTGATTACAG
ΔWAVE1 Reverse + Linker	GGAACCGCCACCACTCCCGCCACCGGATATTGCTTCCAGTAGCACACTCCTGGCATCACTGATTACAG
eGFP Forward	TCCGGTGGCGGGAGTGGTGGCGGTTCCAGCAAGGGCGAGGAGCTGTT
eGFP Reverse	TTCATTACTTGTACAGCTCGTCCATGCC

605

606 In ovo electroporation

607 Fertilised chicken eggs were incubated at 38 °C to stage HH 10-12 and the neural
608 tube was electroporated with a single or combination of constructs at concentrations given in Table 2.
609 We targeted the neural tube region posterior to the forelimb level and along the dorso-ventral
610 axis, transfected cells were typically located throughout the dorsal region and extended to include
611 the Olig2-positive ventral domain. To obtain mosaic expression pattern, neural tubes
612 were electroporated with three 50ms pulses, separated between them with a 950ms gap, at 17 Volts
613 using the ECM 830 square wave electroporation system (BTX).

614

615 Table 2- Plasmid constructs, source and dilution

616

Plasmid	Source	Dilution
pm-eGFP	Tim Sanders, University of Chicago	50 – 100 ng/µl
pm-mKate2	Tim Sanders, University of Chicago	50 – 100 ng/µl
F-tractin-mKate2	Tim Sanders, University of Chicago	50 ng/µl
EB3-sfGFP	Tim Sanders, University of Chicago	25 ng/µl
WAVE1-eGFP	See cloning protocol	1 µg/µl
ΔWAVE1-eGFP	See cloning protocol	1 µg/µl
MyoX-eGFP	Tim Sanders, University of Chicago	1 µg/µl
mNeonGreen-ENA	Allele Biotechnology	1 µg/µl
mNeonGreen-Vasp	Allele Biotechnology	1 µg/µl
mNeonGreen-TOMM20	Allele Biotechnology	1 µg/µl

617

618

619 Embryonic tissue explant culture

620 Electroporated embryos were allowed to develop overnight to stage HH17-18 and the neural tube in
621 the interlimb region was then bisected along the dorsovental axis, to gain access to
622 the neuroepithelial apical surface. The non-electroporated side was discarded and hemi neural tube
623 explants (~ 2-3 somite lengths), including associated somites, were embedded for enface imaging, with
624 the neuroepithelial apical side orientated to face the base of the culture dish. In most experiments only
625 one explant per embryo was used. Explants were embedded in collagen (supplemented with 0.1% acetic
626 acid, 5x L-15 medium [ThermoFisher, 41300] and 7.5% sodium bicarbonate [ThermoFisher, 25080094])
627 in poly-D-lysine coated glass-bottomed petri-dishes (World Precision Instruments, FD35-PDL-
628 100), covered with neurobasal media, supplemented with B-27 (ThermoFisher,
629 17504044), glutamax (ThermoFisher, 35050038) and gentamicin (ThermoFisher, 15750037). The plates
630 were then placed in a 37°C-maintained incubator supplied with 5% CO_2, giving time for the explants to
631 recover for two hours before commencing live imaging (Das et al., 2012).

632

633

634 Time lapse imaging

635 Time-lapse imaging of neural tube explants was performed using a Deltavision Core microscope system
636 in a WeatherStation environmental chamber maintained at 37°C. (GE Healthcare). Imaging was
637 optimised for minimal light transmission, exposure times (50–100 milliseconds) and total acquisition
638 times of 10-20 minutes, to avoid phototoxicity (Das et al., 2012; Das and Storey, 2014). Image
639 acquisition was performed using an Olympus 60 × 1.42 NA oil immersion objective or an Olympus 40 ×
640 1.25 NA silicone oil immersion objective, a solid-state LED light source and a CoolSnap HQ2 cooled CCD
641 camera (Photometrics). Unless otherwise stated, 10 optical sections spaced 0.5 µm apart were acquired
642 for each explant (1024 × 1024 pixels, 1 × 1 binning). For the live imaging sessions totalling for 1 hour,
643 image acquisition between timepoints was set at 1-minute intervals. Images were deconvolved using
644 the SoftWorx image processing software.

645

646 Preparation of tissue for imaging cytoskeletal manipulations

647 To investigate the effect of actin polymerisation inhibition or microtubule stabilisation, neural tube
648 explants embedded for enface imaging were incubated in pre-warmed neurobasal medium
649 containing latrunculin-A (1 µM, Abcam, ab144290) or Taxol (10 µM, Sigma, T7191) for 1 hour before
650 imaging.

651

652 Confocal imaging and 3D modelling

653 Imaging of sections or embedded tissue (Figures 8A, B & D) was carried out with the Leica SP8 confocal
654 microscope (lenses HC PL APO CS2 20x/0.75 DRY or HC PL APO CS2 63x/1.40 OIL). 3D modelling for
655 Movie 7 was carried out using the IMARIS software (Oxford instruments).

656

657 Immunofluorescence and fixed tissue imaging

658 The interlimb region of HH17–18 chick embryos was fixed in 4% paraformaldehyde for 2 hours at 4°C,
659 washed with PBS and equilibrated overnight in 30% sucrose at 4°C. The tissue was then embedded in
660 1.5% LB agar (Sigma, L7025) and 5% sucrose dissolved in PBS. Mounted tissue was dehydrated
661 for 48 hours in 30% sucrose and snap frozen on dry ice. 20-25 µm thick transverse sections were then
662 collected using a Leica cryostat (maintained at −25°C). For immunofluorescence experiments, sections
663 were re-hydrated in 0.1% Triton-X-100/PBS, incubated in blocking buffer for 1-2 hours at room
664 temperature (0.1% Triton-X-100% and 1% heat inactivated donkey and goat serum, in PBS) and
665 incubated overnight with primary antibodies (diluted in blocking buffer) as in Table 3. Sections were
666 washed with 0.1% Triton-X-100/PBS and incubated overnight with secondary antibodies for 2 hours at
667 room temperature. Following washes with 0.1% Triton-X-100/PBS, the sections were mounted in
668 Prolong Gold antifade mountant (ThermoFisher, P36930). For enface imaging of fixed tissue, explants

669 were mounted in 0.5% low gelling temperature agarose (Sigma, A9045). For enface confocal
670 imaging following a live imaging session, the neurobasal medium was immediately replaced with 4%
671 paraformaldehyde for ~1 hour, washed and maintained in PBS. DAPI was added in the PBS washes to
672 stain the nuclei.
673
674 Table 3 Antibodies, stains, sources and dilutions
675

Antibody	Source	Catalogue number	Dilution
Primary antibodies			
Rat N-Cadherin	ThermoFisher	132100	1/300
Tuj1	Biolegend	801213	1/500
Mouse HuC/HuD	ThermoFisher	A21271	1/200
Goat GFP	Abcam	6673	1/500
Sheep Dll1	R&D	AF3970	1/75
Donkey anti-rat 568	Abcam	ab175475	1/300
Secondary antibodies			
Donkey anti- mouse 568	ThermoFisher	A-10037	1/300
Donkey anti- mouse 647	ThermoFisher	A-31571	1/300
Donkey anti-goat 488	ThermoFisher	A-11055	1/300
Donkey anti-sheep 488	ThermoFisher	A-11015	1/300
Phalloidin CF640R	Biotum	00050	1/300

676
677
678 EM sample preparation
679 Chicken embryonic spinal cord at HH12 was fixed in 1% paraformaldehyde and 1.5% glutaraldehyde in
680 0.05 M cacodylate buffer (pH 7.0) for two hours at room temperature and was post-fixed with 1%
681 osmium tetroxide (OsO4). After washing in cacodylate buffer the tissue was stained with 1% tannic acid
682 in 0.1M cacodylate buffer for 1hr. The tissue was then dehydrated through an alcohol series finishing in
683 propylene oxide. The tissue was then infiltrated with Durcupan epoxy resin (Sigma), sectioned with a
684 Leica UCT ultramicrotome and imaged on a FEI Tecnai TEM using the SIS Megaview II CCD camera
685 (Figures 1A-C). Human embryonic tissue fixed in 4% paraformaldehyde and 2.5% glutaraldehyde in
686 0.1M sodium cacodylate buffer (pH 7.2) for 60 minutes was provided by the HDBR. The tissue was
687 washed twice in cacodylate buffer, and small pieces of spinal cord were then post-fixed in 1% OsO4 with
688 1.5% Na ferricyanide in cacodylate buffer for 60 min. After another cacodylate buffer wash they were
689 contrasted with 1% tannic acid and 1% uranyl acetate. The cell pellets were then serially dehydrated
690 into 100% ethanol, changed to propylene oxide left overnight in 50% propylene oxide 50% resin and
691 finally embedded in 100% Durcupan resin (Sigma). The resin was polymerised at 60°C for 48hrs and
692 sectioned on a Leica UCT ultramicrotome. Sections were contrasted with 3% aq uranyl acetate and

693 Reynolds lead citrate before imaging on a JEOL 1200EX TEM using a SIS III camera. Chick embryonic
694 tissue imaged in Supplementary figure3 was prepared using the same protocol as for human tissue.
695
696 Tissue integrity assay using fluorescent dextran
697 Chick embryos were electroporated with pm-eGFP or ΔWAVE1-eGFP at HH10-12 as above and at stage
698 HH17-18, the 70kDa TxRd-tagged Dextran, lysine fixable (ThermoFisher, D1864) (reconstituted
699 following manufacturer's instructions) was injected into the neural tube lumen. Embryos were
700 incubated for an hour and then dissected and fixed immediately with cold 4% PFA, followed by gentle
701 washing in PBS to remove the excess dextran, embedding and cryo-sectioning prior to confocal imaging
702 (as above).
703
704 Software for quantification and analysis
705 The Softworx software (Applied Precision, Inc), was used for the quantifications in Figure 2B, 2D, 3A, 3B,
706 3C, 3D, 3F, 4A, and supplementary figure 1B. Fiji software (Schindelin et al., 2012) was used for the
707 quantifications in Figures 3F, 6B, 6C, 6D, 7B, 7F, 8D, 8F, supplementary figures 1A, 2A and 2C. Results of
708 statistical analyses undertaken using Prism 8 are presented in figure legends, full data and analysis is
709 provided in metadata files.
710
711 Metadata files
712 Figure 2B_Microvilli_and_Lamellipodia.xls
713 Figure 2D_Surface protrusions.xls
714 Figure 3A-B and Supplementary 1B.xls
715 Figure 3C-D and Supplementary 1C
716 Figure 6B – D Lateral filopodia.xls
717 Figure 6C and 7B- Lateral filopodia quantifications.xlsx
718 Figure 7F_Quantification of round-ended apical endfoot phenotype.xls
719 Figure 8D- Lateral protrusions in differentiating Tuj1 positive cells.xlsx
720 Figure 8F- HuCD calculations.xlsx
721 Supplementary Figure 1A- Apical endfoot diameter
722 Supplementary Figure 2A- EB3-sfGFP_pm-mKate2.xlsx
723 Supplementary Figure 2B- EB3-sfGFP_F-tractin-mKate2-log-files.xlsx
724 Supplementary Figure 2E.xls
725

Movie legends

Movies 1, 2: Microvilli (movie 1) and lamellipodial (movie 2) formation at the apical cell membrane. These movies are related to Figure 2A. Mis-expressed pm-eGFP labels the plasma membrane and F-tractin-mKate2 the actin cytoskeleton. Maximum intensity projections of deconvolved image sequences were used. Images acquired every 8 seconds.

Movie 3: Microvilli formation at the apical cell membrane. This movie is related to Figure 2A. Apico-basal Z-stack series across the apical plasma membrane, labelled with pm-eGFP, sub-apical N-Cadherin based adherens junctions (white) help define apico-basal position.

Movie 4: Long thin protrusions extending into the lumen exhibiting retrograde movement of membrane particles. This movie is related to Figure 1C. Mis-expressed pm-eGFP labels the plasma membrane and F-tractin-mKate2 the actin cytoskeleton. Maximum intensity projections of deconvolved image sequences were used. Images acquired every 7 seconds.

Movie 5: Sub-apical lateral protrusions arise beneath the N-Cadherin based adherens junctions. Apico-basal Z-stack series across the apical plasma membrane, labelled with pm-eGFP, sub-apical N-Cadherin (pink) based adherens junctions and nuclei (DAPI, blue).

Movie 6: Sub-apical lateral protrusion dynamics. This movie is related to Figure 2F. Mis-expressed pm-eGFP labels the plasma membrane. Maximum intensity projections of deconvolved image sequences were used. Images acquired every 5 seconds.

Movie 7: A variety of lateral protrusion dimensions revealed by confocal imaging and 3D models. This movie is related to Supplementary Figure 1A. On the left, apico-basal Z-stack series across the apical plasma membrane and on the right a 3D model projection from the former imaging. Mis-expressed pm-eGFP labels the plasma membrane.

Movie 8, 9: Contact of lateral protrusions from non-neighbouring apical endfeet. These movies are related to Figure 3E. Mis-expressed pm-eGFP labels the plasma membrane. Maximum intensity projections of deconvolved image sequences were used. Images acquired every 5 seconds.

Movie 10: Sub-apical protrusions extended around the plasma membrane of neighbouring endfeet. This movie is related to Figure 4C. Mis-expressed pm-eGFP and pm-mKate2 label the plasma membrane. Maximum intensity projections of deconvolved image sequences were used. Images acquired every 15 seconds.

Movie 11, 12: Lateral protrusions from non-neighbouring apical endfeet meet tip to tip and extend along each other. These movies are related to Figures 4D,E. Mis-expressed pm-eGFP and pm-mKate2 label the plasma membrane. Maximum intensity projections of deconvolved image sequences were used. Images acquired every 10 or 15 seconds.

Movie 13: Lateral protrusions contain actin. This movie is related to Figure 5A. Mis-expressed pm-eGFP labels the plasma membrane and F-tractin-mKate2 the actin cytoskeleton. Maximum intensity projections of deconvolved image sequences were used. Images acquired every 8 seconds.

Movie 14: Microtubule growth in lateral protrusions is unidirectional. This movie is related to Figure 5B. Mis-expressed pm-mKate2 labels the plasma membrane and EB3-sfGFP the polymerizing microtubules. Maximum intensity projections of deconvolved image sequences were used. Images acquired every 6 seconds.

Movie 15, 16: mNeonGreen-ENAH or mNeonGreen-VASP localize at adherens junctions. These movies are related to Supplementary Figure 2D. Mis-expressed F-tractin-mKate2 labels the actin cytoskeleton. Maximum intensity projections of deconvolved image sequences were used. Images acquired every 10 seconds.

Movie 17, 18: mNeonGreen-ENAH or mNeonGreen-VASP localize at lateral protrusions. These movies are related to Figure 5C. Mis-expressed F-tractin-mKate2 labels the actin cytoskeleton. Maximum intensity projections of deconvolved image sequences were used. Images acquired every 10 seconds.

Movie 19: Myosin X (MyoX-eGFP) does not localise to lateral protrusion tips. This movie is related to Supplementary Figure 2F. Mis-expressed pm-mKate2 labels the plasma membrane. Maximum intensity projections of deconvolved image sequences were used. Images acquired every 10 seconds.

Movies 20, 21: Thin filopodia extend from lateral protrusions. These movies are related to Figure 6A. Mis-expressed pm-eGFP labels the plasma membrane. Maximum intensity projections of deconvolved image sequences were used. Images acquired every 1 minute.

Movie 22: No mitochondrial transfer between cells through the lateral protrusions. This movie is related to Supplementary Figures 3A, B. Mis-expressed mNeonGreen-TOMM20 labels the mitochondria and pm-mKate2 the plasma membrane. Maximum intensity projections of deconvolved image sequences were used. Images acquired every 10 seconds.

Movies 23-25: Formation of lateral protrusions depend on actin but not microtubules. These movies are related to Figure 7A (movie 2, DMSO control, movie 24 LatA treated; Movie 25 Taxol treated). Mis-expressed pm-eGFP labels the plasma membrane. Maximum intensity projections of deconvolved image sequences were used. Images acquired every 5 seconds.

Movies 26, 27: Lateral protrusions following mis-expression of full length WAVE1-eGFP (movie 26) or mutant WAVE1-eGFP (movie 27), the latter exhibiting a round ended apical endfoot phenotype. These movies are related to Figure 7E. Mis-expressed pm-mKate2 labels the plasma membrane. Maximum intensity projections of deconvolved image sequences were used. Images acquired every 1 minute.

Movie 28: Tuj1 negative progenitors have long lateral protrusions. This movie is related to Figure 8B. Apico-basal Z-stack series across the apical plasma membrane, labelled with pm-eGFP and Tuj1 (left) or pm-eGFP, Tuj1 and N-Cadherin (right).

Movie 29: Tuj1 positive neurons have short lateral protrusions. This movie is related to Figure 8B. Apico-basal Z-stack series across the apical plasma membrane, labelled with pm-eGFP and Tuj1 (left) or pm-eGFP, Tuj1 and N-Cadherin (right).

References

Aaku-Saraste, E., Hellwig, A., Huttner, W.B., 1996. Loss of occludin and functional tight junctions, but not ZO-1, during neural tube closure--remodeling of the neuroepithelium prior to neurogenesis. Dev. Biol. 180, 664–679. https://doi.org/10.1006/dbio.1996.0336

Biga V, Hawley J, Soto X, Johns E, Han D, Bennett H, Adamson AD, Kursawe J, Glendinning P, Manning CS, Papalopulu N 2021 A dynamic, spatially periodic, micro-pattern of HES5 underlies neurogenesis in the mouse spinal cord. Mol. Syst. Biol. 17, e9902. https://doi.org/10.15252/msb.20209902

Boczkowska, M., Rebowski, G., Kast, D.J., Dominguez, R., 2014. Structural analysis of the transitional state of Arp2/3 complex activation by two actin-bound WCAs. Nat. Commun. 5, 3308. https://doi.org/10.1038/ncomms4308

Briscoe, J., Small, S., 2015. Morphogen rules: design principles of gradient-mediated embryo patterning. Dev. Camb. Engl. 142, 3996–4009. https://doi.org/10.1242/dev.129452

Camargo Ortega, G., Falk, S., Johansson, P.A., Peyre, E., Broix, L., Sahu, S.K., Hirst, W., Schlichthaerle, T., De Juan Romero, C., Draganova, K., Vinopal, S., Chinnappa, K., Gavranovic, A., Karakaya, T., Steininger, T., Merl-Pham, J., Feederle, R., Shao, W., Shi, S.-H., Hauck, S.M., Jungmann, R., Bradke, F., Borrell, V., Geerlof, A., Reber, S., Tiwari, V.K., Huttner, W.B., Wilsch-Bräuninger, M., Nguyen, L., Götz, M., 2019. The centrosome protein AKNA regulates neurogenesis via microtubule organization. Nature 567, 113–117. https://doi.org/10.1038/s41586-019-0962-4

Campellone, K.G., Welch, M.D., 2010. A nucleator arms race: cellular control of actin assembly. Nat. Rev. Mol. Cell Biol. 11, 237–251. https://doi.org/10.1038/nrm2867

Carlier, M.-F., Pernier, J., Montaville, P., Shekhar, S., Kühn, S., Cytoskeleton Dynamics and Motility group, 2015. Control of polarized assembly of actin filaments in cell motility. Cell. Mol. Life Sci. CMLS 72, 3051–3067. https://doi.org/10.1007/s00018-015-1914-2

Chen, X.J., Squarr, A.J., Stephan, R., Chen, B., Higgins, T.E., Barry, D.J., Martin, M.C., Rosen, M.K., Bogdan, S., Way, M., 2014. Ena/VASP proteins cooperate with the WAVE complex to regulate the actin cytoskeleton. Dev. Cell 30, 569–584. https://doi.org/10.1016/j.devcel.2014.08.001

Cohen, M., Georgiou, M., Stevenson, N.L., Miodownik, M., Baum, B., 2010. Dynamic filopodia transmit intermittent Delta-Notch signaling to drive pattern refinement during lateral inhibition. Dev. Cell 19, 78–89. https://doi.org/10.1016/j.devcel.2010.06.006

Coué, M., Brenner, S.L., Spector, I., Korn, E.D., 1987. Inhibition of actin polymerization by latrunculin A. FEBS Lett. 213, 316–318. https://doi.org/10.1016/0014-5793(87)81513-2

Damiano-Guercio, J., Kurzawa, L., Mueller, J., Dimchev, G., Schaks, M., Nemethova, M., Pokrant, T., Brühmann, S., Linkner, J., Blanchoin, L., Sixt, M., Rottner, K., Faix, J., 2020. Loss of Ena/VASP interferes with lamellipodium architecture, motility and integrin-dependent adhesion. eLife 9, e55351. https://doi.org/10.7554/eLife.55351

Das, R.M., Storey, K.G., 2014. Apical abscission alters cell polarity and dismantles the primary cilium during neurogenesis. Science 343, 200–204. https://doi.org/10.1126/science.1247521

Das, R.M., Wilcock, A.C., Swedlow, J.R., Storey, K.G., 2012. High-resolution live imaging of cell behavior in the developing neuroepithelium. J. Vis. Exp. JoVE. https://doi.org/10.3791/3920

De Joussineau, C., Soulé, J., Martin, M., Anguille, C., Montcourrier, P., Alexandre, D., 2003. Delta-promoted filopodia mediate long-range lateral inhibition in Drosophila. Nature 426, 555–559. https://doi.org/10.1038/nature02157

Demontis, F., Dahmann, C., 2007. Apical and lateral cell protrusions interconnect epithelial cells in live Drosophila wing imaginal discs. Dev. Dyn. Off. Publ. Am. Assoc. Anat. 236, 3408–3418. https://doi.org/10.1002/dvdy.21324

Dent, E.W., Kwiatkowski, A.V., Mebane, L.M., Philippar, U., Barzik, M., Rubinson, D.A., Gupton, S., Van Veen, J.E., Furman, C., Zhang, J., Alberts, A.S., Mori, S., Gertler, F.B., 2007. Filopodia are required for cortical neurite initiation. Nat. Cell Biol. 9, 1347–1359. https://doi.org/10.1038/ncb1654

Falo-Sanjuan, J., Bray, S.J., 2021. Membrane architecture and adherens junctions contribute to strong Notch pathway activation. Dev. Camb. Engl. 148, dev199831. https://doi.org/10.1242/dev.199831

Farquhar, M.G., Palade, G.E., 1965. Cell junctions in amphibian skin. J. Cell Biol. 26, 263–291. https://doi.org/10.1083/jcb.26.1.263

Gallop, J.L., 2020. Filopodia and their links with membrane traffic and cell adhesion. Semin. Cell Dev. Biol. 102, 81–89. https://doi.org/10.1016/j.semcdb.2019.11.017

Georgiou, M., Baum, B., 2010. Polarity proteins and Rho GTPases cooperate to spatially organise epithelial actin-based protrusions. J. Cell Sci. 123, 1089–1098. https://doi.org/10.1242/jcs.060772

Gerdes, H.-H., Pepperkok, R., 2013. Cell-to-cell communication: current views and future perspectives. Cell Tissue Res. 352, 1–3. https://doi.org/10.1007/s00441-013-1590-1

González-Méndez, L., Gradilla, A.-C., Guerrero, I., 2019. The cytoneme connection: direct long-distance signal transfer during development. Dev. Camb. Engl. 146, dev174607. https://doi.org/10.1242/dev.174607

Hadjivasiliou, Z., Moore, R.E., McIntosh, R., Galea, G.L., Clarke, J.D.W., Alexandre, P., 2019. Basal Protrusions Mediate Spatiotemporal Patterns of Spinal Neuron Differentiation. Dev. Cell 49, 907-919.e10. https://doi.org/10.1016/j.devcel.2019.05.035

Hatakeyama, J., Wakamatsu, Y., Nagafuchi, A., Kageyama, R., Shigemoto, R., Shimamura, K., 2014. Cadherin-based adhesions in the apical endfoot are required for active Notch signaling to control neurogenesis in vertebrates. Development 141, 1671–1682. https://doi.org/10.1242/dev.102988

Hatta, K., Takeichi, M., 1986. Expression of N-cadherin adhesion molecules associated with early morphogenetic events in chick development. Nature 320, 447–449. https://doi.org/10.1038/320447a0

Henrique, D., Adam, J., Myat, A., Chitnis, A., Lewis, J., Ish-Horowicz, D., 1995. Expression of a Delta homologue in prospective neurons in the chick. Nature 375, 787–790. https://doi.org/10.1038/375787a0

Henrique, D., Schweisguth, F., 2019. Mechanisms of Notch signaling: a simple logic deployed in time and space. Dev. Camb. Engl. 146, dev172148. https://doi.org/10.1242/dev.172148

927 Hsiung, F., Ramirez-Weber, F.-A., Iwaki, D.D., Kornberg, T.B., 2005. Dependence of Drosophila wing
928 imaginal disc cytonemes on Decapentaplegic. Nature 437, 560–563.
929 https://doi.org/10.1038/nature03951
930
931 Huang, H., Liu, S., Kornberg, T.B., 2019. Glutamate signaling at cytoneme synapses. Science 363, 948–
932 955. https://doi.org/10.1126/science.aat5053
933
934 Ito, Y., Carss, K.J., Duarte, S.T., Hartley, T., Keren, B., Kurian, M.A., Marey, I., Charles, P., Mendonça, C.,
935 Nava, C., Pfundt, R., Sanchis-Juan, A., van Bokhoven, H., van Essen, A., van Ravenswaaij-Arts, C., NIHR
936 BioResource, Care4Rare Canada Consortium, Boycott, K.M., Kernohan, K.D., Dyack, S., Raymond, F.L.,
937 2018. De Novo Truncating Mutations in WASF1 Cause Intellectual Disability with Seizures. Am. J. Hum.
938 Genet. 103, 144–153. https://doi.org/10.1016/j.ajhg.2018.06.001
939
940 Itoh, Y., Moriyama, Y., Hasegawa, T., Endo, T.A., Toyoda, T., Gotoh, Y., 2013. Scratch regulates
941 neuronal migration onset via an epithelial-mesenchymal transition-like mechanism. Nat. Neurosci. 16,
942 416–425. https://doi.org/10.1038/nn.3336
943
944 Kadowaki, M., Nakamura, S., Machon, O., Krauss, S., Radice, G.L., Takeichi, M., 2007. N-cadherin
945 mediates cortical organization in the mouse brain. Dev. Biol. 304, 22–33.
946 https://doi.org/10.1016/j.ydbio.2006.12.014
947
948 Kasioulis, I., Das, R.M., Storey, K.G., 2017. Inter-dependent apical microtubule and actin dynamics
949 orchestrate centrosome retention and neuronal delamination. eLife 6.
950 https://doi.org/10.7554/eLife.26215
951
952 Kasioulis, I., Storey, K.G., 2018. Cell biological mechanisms regulating chick neurogenesis. Int. J. Dev.
953 Biol. 62, 167–175. https://doi.org/10.1387/ijdb.170268ks
954
955 Kawaguchi, A., 2020. Neuronal Delamination and Outer Radial Glia Generation in Neocortical
956 Development. Front. Cell Dev. Biol. 8, 623573. https://doi.org/10.3389/fcell.2020.623573
957
958 Korenkova, O., Pepe, A., Zurzolo, C., 2020. Fine intercellular connections in development: TNTs,
959 cytonemes, or intercellular bridges? Cell Stress 4, 30–43. https://doi.org/10.15698/cst2020.02.212
960
961 Kornberg, T.B., 2014. Cytonemes and the dispersion of morphogens. Wiley Interdiscip. Rev. Dev. Biol.
962 3, 445–463. https://doi.org/10.1002/wdev.151
963
964 Kwiatkowski, A.V., Rubinson, D.A., Dent, E.W., Edward van Veen, J., Leslie, J.D., Zhang, J., Mebane,
965 L.M., Philippar, U., Pinheiro, E.M., Burds, A.A., Bronson, R.T., Mori, S., Fässler, R., Gertler, F.B., 2007.
966 Ena/VASP Is Required for neuritogenesis in the developing cortex. Neuron 56, 441–455.
967 https://doi.org/10.1016/j.neuron.2007.09.008
968 Lebrand, C., Dent, E.W., Strasser, G.A., Lanier, L.M., Krause, M., Svitkina, T.M., Borisy, G.G., Gertler,
969 F.B., 2004. Critical role of Ena/VASP proteins for filopodia formation in neurons and in function
970 downstream of netrin-1. Neuron 42, 37–49. https://doi.org/10.1016/s0896-6273(04)00108-4
971
972 Leerberg, J.M., Gomez, G.A., Verma, S., Moussa, E.J., Wu, S.K., Priya, R., Hoffman, B.D., Grashoff, C.,
973 Schwartz, M.A., Yap, A.S., 2014. Tension-sensitive actin assembly supports contractility at the
974 epithelial zonula adherens. Curr. Biol. CB 24, 1689–1699. https://doi.org/10.1016/j.cub.2014.06.028
975
976 Li, J.X.H., Tang, V.W., Boateng, K.A., Brieher, W.M., 2021. Cadherin puncta are interdigitated dynamic
977 actin protrusions necessary for stable cadherin adhesion. Proc. Natl. Acad. Sci. U. S. A. 118,
978 e2023510118. https://doi.org/10.1073/pnas.2023510118

Li, J.X.H., Tang, V.W., Brieher, W.M., 2020. Actin protrusions push at apical junctions to maintain E-cadherin adhesion. Proc. Natl. Acad. Sci. U. S. A. 117, 432–438. https://doi.org/10.1073/pnas.1908654117

Luz, M., Spannl-Müller, S., Özhan, G., Kagermeier-Schenk, B., Rhinn, M., Weidinger, G., Brand, M., 2014. Dynamic association with donor cell filopodia and lipid-modification are essential features of Wnt8a during patterning of the zebrafish neuroectoderm. PloS One 9, e84922. https://doi.org/10.1371/journal.pone.0084922

Marzesco, A.-M., Janich, P., Wilsch-Bräuninger, M., Dubreuil, V., Langenfeld, K., Corbeil, D., Huttner, W.B., 2005. Release of extracellular membrane particles carrying the stem cell marker prominin-1 (CD133) from neural progenitors and other epithelial cells. J. Cell Sci. 118, 2849–2858. https://doi.org/10.1242/jcs.02439

Mattes, B., Dang, Y., Greicius, G., Kaufmann, L.T., Prunsche, B., Rosenbauer, J., Stegmaier, J., Mikut, R., Özbek, S., Nienhaus, G.U., Schug, A., Virshup, D.M., Scholpp, S., 2018. Wnt/PCP controls spreading of Wnt/β-catenin signals by cytonemes in vertebrates. eLife 7, e36953. https://doi.org/10.7554/eLife.36953

Mattes, B., Scholpp, S., 2018. Emerging role of contact-mediated cell communication in tissue development and diseases. Histochem. Cell Biol. 150, 431–442. https://doi.org/10.1007/s00418-018-1732-3

Meng, W., Takeichi, M., 2009. Adherens junction: molecular architecture and regulation. Cold Spring Harb. Perspect. Biol. 1, a002899. https://doi.org/10.1101/cshperspect.a002899

Miki, H., Suetsugu, S., Takenawa, T., 1998. WAVE, a novel WASP-family protein involved in actin reorganization induced by Rac. EMBO J. 17, 6932–6941. https://doi.org/10.1093/emboj/17.23.6932

Miyata, T., 2008. Development of three-dimensional architecture of the neuroepithelium: role of pseudostratification and cellular “community.” Dev. Growth Differ. 50 Suppl 1, S105-112. https://doi.org/10.1111/j.1440-169X.2007.00980.x

Moore, R.E., Clarke, J., Alexandre, P., 2020. Protrusion-Mediated Signaling Regulates Patterning of the Developing Nervous System. Front. Cell Dev. Biol. 8, 579073. https://doi.org/10.3389/fcell.2020.579073

Nelson, B.R., Hodge, R.D., Bedogni, F., Hevner, R.F., 2013. Dynamic interactions between intermediate neurogenic progenitors and radial glia in embryonic mouse neocortex: potential role in Dll1-Notch signaling. J. Neurosci. Off. J. Soc. Neurosci. 33, 9122–9139. https://doi.org/10.1523/JNEUROSCI.0791-13.2013

Paridaen, J.T.M.L., Huttner, W.B., 2014. Neurogenesis during development of the vertebrate central nervous system. EMBO Rep. 15, 351–364. https://doi.org/10.1002/embr.201438447

Parrini, E., Conti, V., Dobyns, W.B., Guerrini, R., 2016. Genetic Basis of Brain Malformations. Mol. Syndromol. 7, 220–233. https://doi.org/10.1159/000448639

Pollard, T.D., Borisy, G.G., 2003. Cellular motility driven by assembly and disassembly of actin filaments. Cell 112, 453–465. https://doi.org/10.1016/s0092-8674(03)00120-x

1029 Rajan, A., Tien, A.-C., Haueter, C.M., Schulze, K.L., Bellen, H.J., 2009. The Arp2/3 complex and WASp
1030 are required for apical trafficking of Delta into microvilli during cell fate specification of sensory organ
1031 precursors. Nat. Cell Biol. 11, 815–824. https://doi.org/10.1038/ncb1888
1032
1033 Ramírez-Weber, F.A., Kornberg, T.B., 1999. Cytonemes: cellular processes that project to the principal
1034 signaling center in Drosophila imaginal discs. Cell 97, 599–607. https://doi.org/10.1016/s0092-
1035 8674(00)80771-0
1036
1037 Robert Manak, J., 2018. Chapter 6 - Planar Cell Polarity and the Cell Biology of Nervous System
1038 Development and Disease, in: Michael Conn, P. (Ed.), Cell Polarity in Development and Disease,
1039 Perspectives in Translational Cell Biology. Academic Press, Boston, pp. 147–176.
1040 https://doi.org/10.1016/B978-0-12-802438-6.00006-1
1041
1042 Rousso, D.L., Pearson, C.A., Gaber, Z.B., Miquelajauregui, A., Li, S., Portera-Cailliau, C., Morrisey, E.E.,
1043 Novitch, B.G., 2012. Foxp-mediated suppression of N-cadherin regulates neuroepithelial character and
1044 progenitor maintenance in the CNS. Neuron 74, 314–330.
1045 https://doi.org/10.1016/j.neuron.2012.02.024
1046
1047 Roy, S., Huang, H., Liu, S., Kornberg, T.B., 2014. Cytoneme-mediated contact-dependent transport of
1048 the Drosophila decapentaplegic signaling protein. Science 343, 1244624.
1049 https://doi.org/10.1126/science.1244624
1050
1051 Rustom, A., Saffrich, R., Markovic, I., Walther, P., Gerdes, H.-H., 2004. Nanotubular highways for
1052 intercellular organelle transport. Science 303, 1007–1010. https://doi.org/10.1126/science.1093133
1053
1054 Sanders, T.A., Llagostera, E., Barna, M., 2013. Specialized filopodia direct long-range transport of SHH
1055 during vertebrate tissue patterning. Nature 497, 628–632. https://doi.org/10.1038/nature12157
1056
1057 Sauer, F.C., 1935. Mitosis in the neural tube. J. Comp. Neurol. 62, 377–405.
1058 https://doi.org/10.1002/cne.900620207
1059
1060 Schiff, P.B., Horwitz, S.B., 1980. Taxol stabilizes microtubules in mouse fibroblast cells. Proc. Natl.
1061 Acad. Sci. U. S. A. 77, 1561–1565. https://doi.org/10.1073/pnas.77.3.1561
1062
1063 Schindelin, J., Arganda-Carreras, I., Frise, E., Kaynig, V., Longair, M., Pietzsch, T., Preibisch, S., Rueden,
1064 C., Saalfeld, S., Schmid, B., Tinevez, J.-Y., White, D.J., Hartenstein, V., Eliceiri, K., Tomancak, P.,
1065 Cardona, A., 2012. Fiji: an open-source platform for biological-image analysis. Nat. Methods 9, 676–
1066 682. https://doi.org/10.1038/nmeth.2019
1067
1068 Sheen, V.L., Dixon, P.H., Fox, J.W., Hong, S.E., Kinton, L., Sisodiya, S.M., Duncan, J.S., Dubeau, F.,
1069 Scheffer, I.E., Schachter, S.C., Wilner, A., Henchy, R., Crino, P., Kamuro, K., DiMario, F., Berg, M.,
1070 Kuzniecky, R., Cole, A.J., Bromfield, E., Biber, M., Schomer, D., Wheless, J., Silver, K., Mochida, G.H.,
1071 Berkovic, S.F., Andermann, F., Andermann, E., Dobyns, W.B., Wood, N.W., Walsh, C.A., 2001.
1072 Mutations in the X-linked filamin 1 gene cause periventricular nodular heterotopia in males as well as
1073 in females. Hum. Mol. Genet. 10, 1775–1783. https://doi.org/10.1093/hmg/10.17.1775
1074
1075 Shepard, T.H., Park, H.W., Pascoe-Mason, J., 1993. Glucose causes lengthening of the microvilli of the
1076 neural plate of the rat embryo and produces a helical pattern on their surface. Teratology 48, 65–74.
1077 https://doi.org/10.1002/tera.1420480111
1078
1079 Shepard, T.H., Tanimura, T., Park, H.W., 1997. Glucose absorption and utilization by rat embryos. Int. J.
1080 Dev. Biol. 41, 307–314.

1081
1082 Shinoda, T., Nagasaka, A., Inoue, Y., Higuchi, R., Minami, Y., Kato, K., Suzuki, M., Kondo, T., Kawaue, T.,
1083 Saito, K., Ueno, N., Fukazawa, Y., Nagayama, M., Miura, T., Adachi, T., Miyata, T., 2018. Elasticity-based
1084 boosting of neuroepithelial nucleokinesis via indirect energy transfer from mother to daughter. PLoS
1085 Biol. 16, e2004426.
1086 https://doi.org/10.1371/journal.pbio.2004426
1087
1088 Smith, M.T., Wood, L.R., Honig, S.R., 1982. Scanning electronmicroscopy of experimental anencephaly
1089 development. Neurology 32, 992–999. https://doi.org/10.1212/wnl.32.9.992
1090 Stanganello, E., Hagemann, A.I.H., Mattes, B., Sinner, C., Meyen, D., Weber, S., Schug, A., Raz, E.,
1091 Scholpp, S., 2015. Filopodia-based Wnt transport during vertebrate tissue patterning. Nat. Commun.
1092 6, 5846. https://doi.org/10.1038/ncomms6846
1093
1094 Sweeney, M.O., Collins, A., Padrick, S.B., Goode, B.L., 2015. A novel role for WAVE1 in controlling actin
1095 network growth rate and architecture. Mol. Biol. Cell 26, 495–505. https://doi.org/10.1091/mbc.E14-
1096 10-1477
1097
1098 Tang, V.W., Brieher, W.M., 2012. α-Actinin-4/FSGS1 is required for Arp2/3-dependent actin assembly
1099 at the adherens junction. J. Cell Biol. 196, 115–130. https://doi.org/10.1083/jcb.201103116
1100
1101 Victoria, G.S., Zurzolo, C., 2017. The spread of prion-like proteins by lysosomes and tunneling
1102 nanotubes: Implications for neurodegenerative diseases. J. Cell Biol. 216, 2633–2644.
1103 https://doi.org/10.1083/jcb.201701047
1104
1105 Waterman, R.E., 1976. Topographical changes along the neural fold associated with neurulation in the
1106 hamster and mouse. Am. J. Anat. 146, 151–171. https://doi.org/10.1002/aja.1001460204
1107
1108 Weigmann, A., Corbeil, D., Hellwig, A., Huttner, W.B., 1997. Prominin, a novel microvilli-specific
1109 polytopic membrane protein of the apical surface of epithelial cells, is targeted to plasmalemmal
1110 protrusions of non-epithelial cells. Proc. Natl. Acad. Sci. U. S. A. 94, 12425–12430.
1111 https://doi.org/10.1073/pnas.94.23.12425
1112
1113 Wolpert, L., 2016. Positional Information and Pattern Formation. Curr. Top. Dev. Biol. 117, 597–608.
1114 https://doi.org/10.1016/bs.ctdb.2015.11.008
1115
1116 Yamazaki, D., Fujiwara, T., Suetsugu, S., Takenawa, T., 2005. A novel function of WAVE in lamellipodia:
1117 WAVE1 is required for stabilization of lamellipodial protrusions during cell spreading. Genes Cells
1118 Devoted Mol. Cell. Mech. 10, 381–392. https://doi.org/10.1111/j.1365-2443.2005.00845.x
1119
1120 Zhang, J., Neal, J., Lian, G., Hu, J., Lu, J., Sheen, V., 2013. Filamin A regulates neuronal migration
1121 through brefeldin A-inhibited guanine exchange factor 2-dependent Arf1 activation. J. Neurosci. Off. J.
1122 Soc. Neurosci. 33, 15735–15746. https://doi.org/10.1523/JNEUROSCI.1939-13.2013
1123
1124 Zhang, J., Woodhead, G.J., Swaminathan, S.K., Noles, S.R., McQuinn, E.R., Pisarek, A.J., Stocker, A.M.,
1125 Mutch, C.A., Funatsu, N., Chenn, A., 2010. Cortical neural precursors inhibit their own differentiation
1126 via N-cadherin maintenance of beta-catenin signaling. Dev. Cell 18, 472–479.
1127 https://doi.org/10.1016/j.devcel.2009.12.025
1128